GREEN SYNTHESIS OF CuO@ZnO NANOCOMPOSITES USING LEAF EXTRACT OF *ARTEMISIA VULGARIS* AND STUDY OF ITS PHOTOCATALYTIC ACTIVITIES

A DISSERTATION WORK SUBMITTED FOR THE PARTIAL FULFILLMENT OF THE REQUIREMENTS FOR THE MASTER OF SCIENCE DEGREE IN CHEMISTRY

SUBMITTED BY

PUJAN NEPAL

TU EXAMINATION ROLL NO.: 1894/ 076

TU Reg. No.: 5-2-0050-125-2015

SUBMITTED TO

DEPARTMENT OF CHEMISTRY

AMRIT CAMPUS

INSTITUTE OF SCIENCE AND TECHNOLOGY

TRIBHUVAN UNIVERSITY

KATHMANDU, NEPAL

June, 2023

BOARD OF EXAMINER AND CERTIFICATE OF APPROVAL

This dissertation entitled "Green synthesis of CuO@ZnO nanocomposites using leaf extract of *Artemisia vulgaris* and study of its photocatalytic activities" by Pujan Nepal under the supervision of Asst. Prof. Dr. Deval Prasad Bhattarai, and Co-supervison of Asst. Prof. Hari Bhakta Oli, Department of Chemistry, Amrit Campus, Tribhuvan University, Kathmandu, Nepal, hereby submitted has been approved for partial fulfillment of the requirement for completion of Master of Science (M.Sc.) Degree in Chemistry. This dissertation has not been submitted to any other university or institution previously for the award of a degree.

.....

Supervisor

Asst. Prof. Dr. Deval Prasad Bhattarai

Department of Chemistry

Amrit Campus, TU, Kathmandu, Nepal

.....

Co-supervisor

Asst. Prof. Hari Bhakta Oli

Department of Chemistry

Amrit Campus, TU, Kathmandu, Nepal

.....

External Examiner

Prof. Dr. Niranjan Parajuli

Central Department of Chemistry

Tribhuvan University, Nepal

.....

Internal Examiner

Prof. Dr. Daman Raj Gautam

Department of Chemistry

Amrit Campus, TU, Nepal

.....

Head of Department

Assoc. Prof. Kanchan Sharma

Department of Chemistry

Amrit Campus, TU, Kathmandu, Nepal

.....

M.Sc. Program Co-ordinator

Assoc. Prof. Dr. Bhushan Shakya

Department of Chemistry

Amrit Campus, TU, Kathmandu, Nepal

Date: July 5, 2023

Tribhuvan University
Amrit Campus
Department of

RECOMMENDATION LETTER

This is to recommend that the dissertation entitled "Green synthesis of CuO@ZnO nanocomposite using leaf extract of *Artemisia vulgaris* and study of its photocatalytic activities" has been carried out by Mr. Pujan Nepal as a partial fulfillment for the requirement of M.Sc. Degree in Chemistry under our supervision and guidance. The work presented herein is genuine and performed originally by Mr. Pujan Nepal and has not been submitted elsewhere for any other degree. He has performed this research work sincerely and satisfactorily. We, therefore, recommend this dissertation for approval and acceptance.

.....

Supervisor

Asst. Prof. Dr. Deval Prasad Bhattarai

Department of Chemistry

Amrit Campus

Tribhuvan University, Nepal

Tribhuvan University
Amrit Campus
Department of Chemistry

.....

Co-supervisor

Asst. Prof. Hari Bhakta Oli

Department of Chemistry

Amrit Campus

Tribhuvan University, Nepal

Date: June 25, 2023

DECLARATION

I, Pujan Nepal, hereby declare that this dissertation entitled "Green synthesis of CuO@ZnO nanocomposite using leaf extract of *Artemisia vulgaris* and study of its photocatalytic activities" being submitted to the Department of Chemistry, Amrit Campus, Institute of Science and Technology (IoST), Tribhuvan University (T.U.), Nepal for the partial fulfillment of the requirement in Master of Science (M.Sc.) Degree in Chemistry is carried out by me under the supervision of Assistant Professor Dr. Deval Prasad Bhattarai. This work is genuine and originally performed by me. It has not been submitted elsewhere for any other degree program. Any literature, data or works done by other researchers are duly cited and acknowledged.

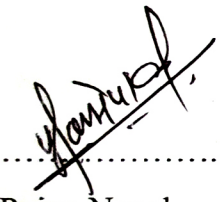

.....

Pujan Nepal

Roll No: 1894/076

T.U. Registration No: 5-2-0050-125-2015

June, 2023

ACKNOWLEDGEMENTS

I would like to express my special thanks of gratitude to my supervisor Asst. Prof. Dr. Deval Prasad Bhattarai for his guidance, support, and supervision in completing this dissertation. I would also like to extend my deepest gratitude to my co-supervisor Asst. Prof. Hari Bhakta Oli for his suggestions, guidance, and insightful comments. Likewise, I would like to thank to the Head of the Department, Assoc. Prof. Kanchan Sharma and M.Sc. Chemistry Co-ordinator Assoc. Prof. Dr. Bhushan Shakya as well as the entire campus team who helped me during my work by providing the laboratory facilities and moral support to conduct my research work. I came to know about so many new things. I am thankful to them. In addition, I want to extend my especial thanks to my colleague Ms. Sandhya Parajuli and Ms. Asmita Thapa Magar for their unconditional support and help, and also I would like to thank Dr. Ganesh Awasthi for his valuable time, cooperation and collaboration regarding characterization of the samples.

I would also like to thank laboratory officers, Mr. Nanda Krishna Manandhar and Mr. Mani Raj Budhathoki for their help during the laboratory work.

Just as importantly, I would also like to thank my parents and friends who helped me a lot in finalizing this work within the limited time frame.

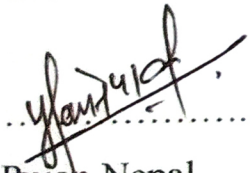

Pujan Nepal

June, 2023

ABSTRACT

In this study, CuO NPs, ZnO NPs, and CuO@ZnO NCs were synthesized by green chemistry approach using the leaves extract of *Artemisia vulgaris*. The Leaves extract was characterized by qualitative chemical tests and spectroscopic measurements. Bioactive compounds present in *Artemisia vulgaris* act as stabilizing and reducing agents. UV-visible spectroscopy, FTIR, EDX, XRD, and FESEM were used to characterize the formation of CuO, ZnO, and CuO@ZnO NPs. XRD pattern revealed the crystalline nature of nanoparticles. The size of CuO NPs, ZnO NPs, and CuO@ZnO NCs were found to be 17.24, 20.74, and 19-24 nm, respectively. The synthesized NPs and NCs were used for the catalytic photodegradation of Methylene blue. The MB was degraded at room temperature under exposure to UV light. The degradation efficiency of CuO, ZnO, and 2 %CuO@ZnO were found to be 52 %, 68 %, and 98 %, respectively. Therefore, it was found that CuO@ZnO nanocomposites have potential to degrade MB as organic dye, and can be used for wastewater treatment.

Keywords: Green chemistry; *Artemisia vulgaris*; CuO@ZnO NCs; Methylene blue; Photocatalytic degradation;

LIST OF ABBREVIATIONS

CuO:	Copper Oxide
ZnO:	Zinc Oxide
NPs:	Nanoparticles
NCs:	Nanocomposites
MB:	Methylene Blue
MO:	Methyl Orange
RhB:	Rhodamine B
CB:	Conduction Band
VB:	Valence Band
eV:	Electron Volt
UV:	Ultra Violet
FT-IR:	Fourier Transform Infrared Spectroscopy
XRD:	X-ray Diffraction
JCPDS:	Joint Committee on Powder Diffraction Standards
EDX:	Energy Dispersive X-ray
FE-SEM:	Field Emission Scanning Electron Microscopy

LIST OF SCHEMES

LISTS OF FIGURES

LIST OF TABLES

TABLE OF CONTENTS

CHAPTER 1
INTRODUCTION

1.1. Background

Nanoscience deals with the study of nanomaterials i.e. materials with a nanomateric dimension (10^{-9} m). Based on their dimension nanomaterials can be further classified into nanoparticles, nanorods, nanotubes, nanosheets, nanofilms, etc. (Neupane, 2018). Whereas nanotechnology seeks to design functional nanomaterials of targeted properties like profound surface area, physical and chemical properties, suitable size distribution, etc. The synthesis of these materials is based on the principle/theory of nanoscience (Aritonang et al., 2019;Ebrahiminezhad et al., 2016;Tahvilian et al., 2019). Because of their tunable properties, nanomaterials can be used in varieties of fields including the environment, food, optics, healthcare, chemical industries, biosensor, medication delivery, cancer therapy, material science and engineering, electrical and communication engineering, computer science and information technology, etc. (Roy, 2017).

Recently, nanotechnology is gaining much attention due to its versatile applications and technological applications though it has insidiously entered into human civilization since immemorial time. The use of nanomaterials and nanoscale formation process dates back to ancient time (Tolochko, 2009). But the credit of nanoscience goes to Richard Feynman, a physicist, because of his to the establishment and generalization of this field (Feynman, 1960). Also, to Nario Taniguchi for his contribution in the field of nanotechnology (Goyal, 2017). In this era of nanotechnology, the discovery of various nanomaterials like carbon nanotubes, fullerenes, and quantum dots with unique mechanical, thermal, and electrical properties have been reported (Alivisatos et al., 1996; Iijima, 1991; Kroto et al., 1985).

Similarly, the development of molecular scale transistors, material designs for targeted drug delivery, nanosensors, etc. have been explored (Tolochko, 2009). Hereafter, this field is mature and multidisciplinary with many practical applications in the areas such as electronics, medicine, energy, and material science.

Ongoing research in nanotechnology continues to explore the possibilities of manipulating materials at the nanoscale and developing new nanomaterials with unique properties.

1.2. Classification of Nanomaterial

Nanomaterials can be classified based on their size, composition, and properties. Here are some commonly recognized categories of nanomaterials with examples.

1.2.1. Classification based on composition

Based on the composition of the nanomaterials they are classified into five types as shown in scheme 1.

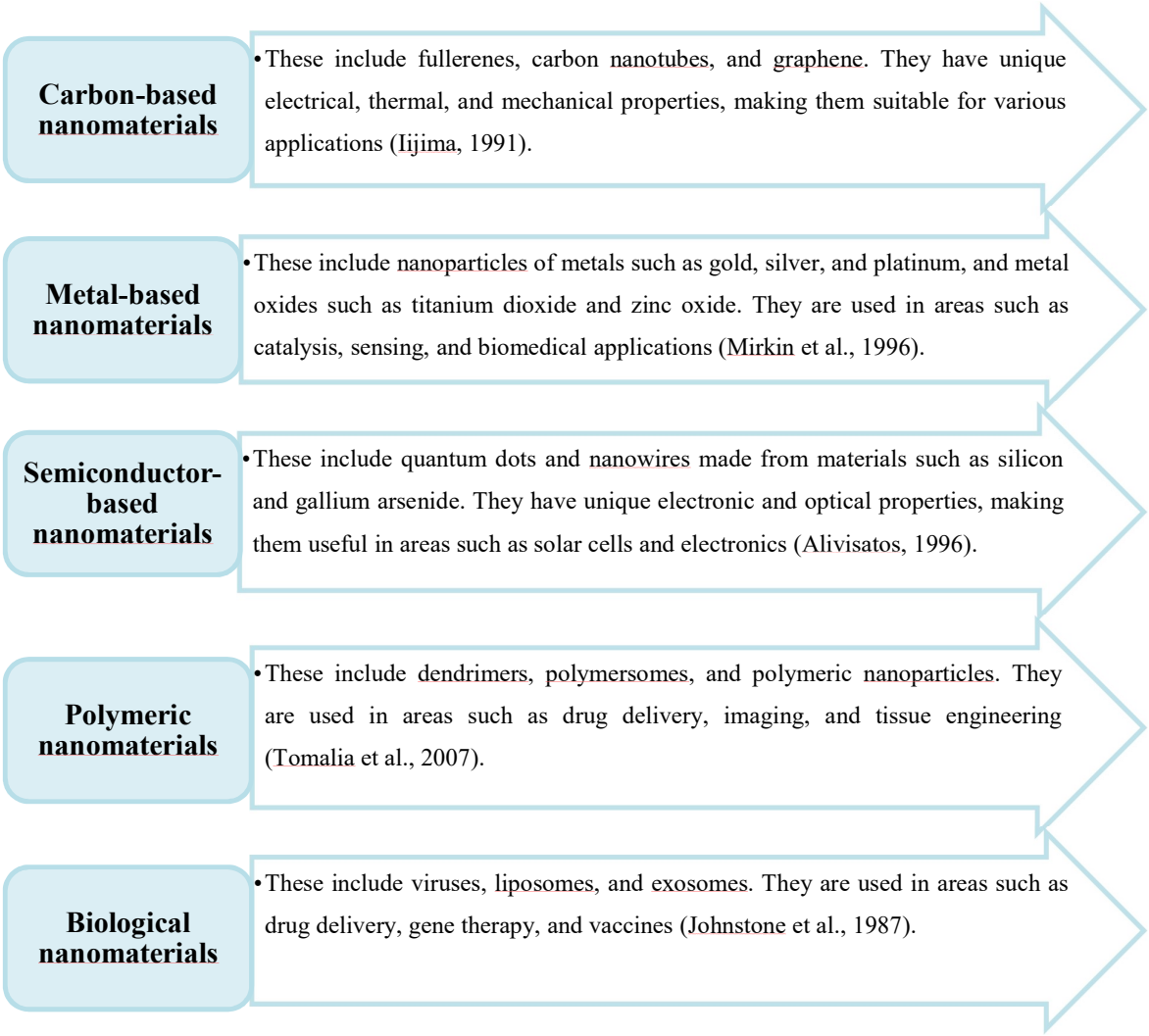

Scheme 1: Classification of nanomaterials based on composition

1.2.2. Classification based on dimensions

Nanomaterials can be classified based on their dimensions into four different classes such as zero dimensional, one dimensional, two dimensional and three dimensional nanomaterials (Kolahalam et al., 2019) shown in scheme 2.

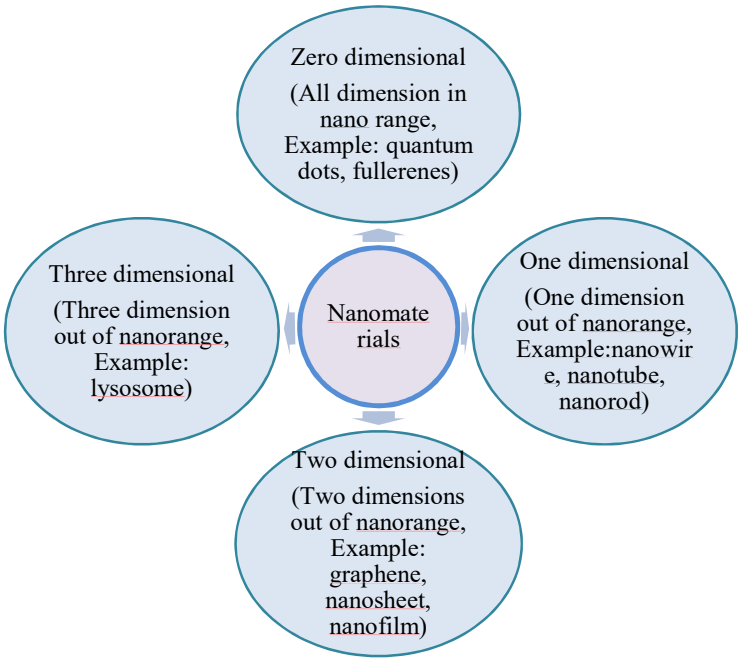

Scheme 2: Classification of nanomaterials based on the dimension

1.3. Synthesis Approaches of Nanomaterials

There are two synthesis approaches categorized as 'top-down' and 'bottom-up' approaches as shown in scheme 3 below.

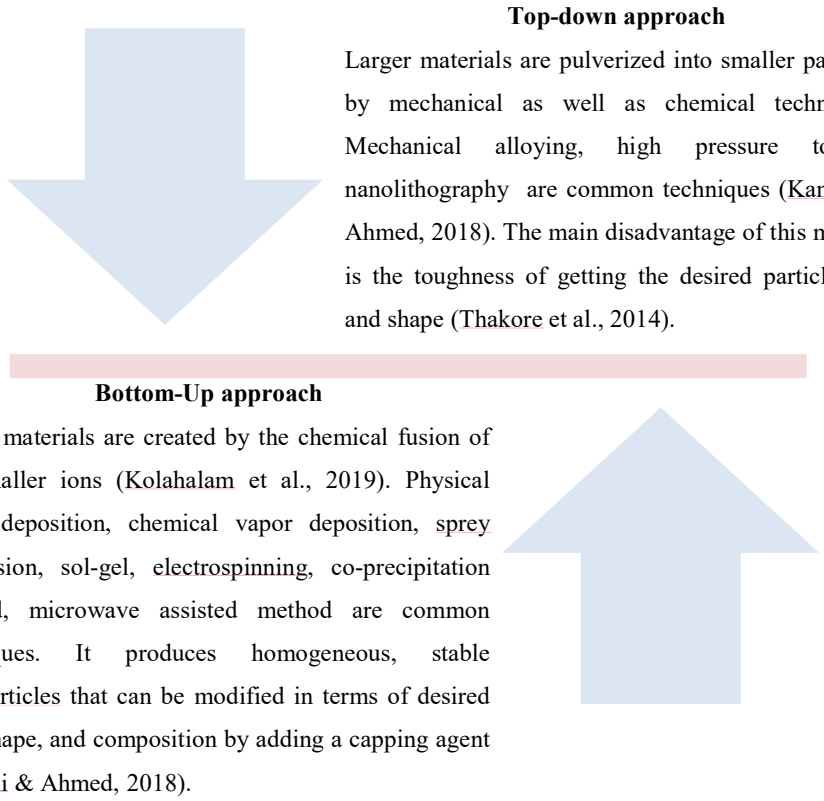

Scheme 3: Top down and bottom up approach

1.4. Green synthesis of nanomaterials

Green synthesis of nanomaterials is the bottom up approach. It is the process of synthesis of nanomaterials by utilizing non-hazardous, renewable, and low-cost materials as raw materials. The main theme of green approach is to find new ways to create the best chemical products and processes by obeying the principle of green chemistry (Anastas & Warner, 1998).

A large-scale manufacturing with minimal contamination has resulted from the synthesis of nanomaterials employing a variety of sources, including bacteria, fungi, algae, and plants, due to the growing popularity of green technologies (Ahmad et al., 2019). Herein, plant extract, microorganisms, biological templates, etc. are used as capping or stabilizing agents (Daphne et al., 2018). Among these, synthesis of nanomaterials using bacteria, fungi, algae, and biological templates are limited because of their super specificity towards nanoparticles. So, in the broad-spectrum synthesis of nanomaterials plant extracts are highly recommended.

Plants are regarded as highly desirable system for nanoparticles range of bioactive secondary metabolites with profound reducing potential (Pandey et al., 2013). The benefit of using plant extract includes not having to go through laborious and expensive steps of growth and storage, safe and ease of scaling up for commercial manufacturing (Kouhbanani et al., 2018). And a notable advantage is that no separate reducing, capping, stabilizing agents are to be added in the whole synthesis process i.e. plant extract itself functions as all (M. Khan et al., 2018; Marslin et al., 2018).

1.5. Green Synthesis of Nanocomposite

A nanocomposite is a composite of two or more nanomaterials, in which one of the components has at least one dimension in nanoscopic size and have special physical and chemical properties (Pandya et al., 2013). As compared to mono metallic nanomaterial, nanocomposites have more reactive sites and are more stable, efficient, and efficacious (Reshmy et al., 2021). There are various methods such as co-precipitation, hydrothermal, sol-gel, chemical vapour deposition, wet impregnation, thermal decomposition, complex directed hybridization, direct heating, electrospinning, microwave synthesis, biosynthesis, etc. for the synthesis of nanocomposite (Das & Srivastava, 2018). However, they are limited due to high cost, toxicity, and accessibility. In this context, green method of nanomaterial synthesis can be the best alternative approach. The synthesis of CuO/ZnO nanocomposites (NCs)

has been described utilizing plant extracts such as *Clerodendrum infortunatum* (S. A. Khan et al., 2018), *Melissa officinalis* L. (Bordbar et al., 2018), *Vaccinium arctostaphylos* L. (Mohammadi-Aloucheh et al., 2018), *Ginkgo biloba* (Thatikayala & Min, 2021), *V. sinaiticum* (Bekru et al., 2022), and *Aegle marmelos* (Basavegowda et al., 2022), bark of *Theobroma cacao* (Yulizar et al., 2018), *Dovyalis caffra* (Adeyemi et al., 2022), *Mentha longifolia* (Fouda et al., 2020) and Nettle leaf (Kalia et al., 2021).

More focused on the synthesis of CuO@ZnO nanocomposites is because of their wide varieties of applications such as catalysts with high activity and specificity, metal semiconductor junctions, thermoelectric effect for applications such as heating air, air conditioning, biomedical devices, military devices, refrigeration, electricity generation, wearable textile, etc. (Bisht et al., 2021), photocatalytic degradation of pollutant, gas sensor, solar cell, H_2 generation, humidity sensor, optoelectronic and magnetic storage devices, other environmental, domestic, and commercial applications (Das & Srivastava, 2018). Among them, the photocatalytic activity of the CuO@ZnO nanocomposites is focused in this study.

1.6. Photocatalytic activity

Photocatalytic activity is the ability of a substance to speed up a chemical reaction by absorbing light energy. Meanwhile, when a photocatalyst material is exposed to light, it can produce electron-hole pairs that trigger redox reactions with molecules that have been adsorbed on its surface or in the surroundings. This beautiful property of the material can be used for degrading contaminants in water. Not limited to this, it can be used to increase the efficiency of solar cells, prepare fuels from carbon dioxide, and produce hydrogen from water (X. Li et al., 2022).

One of the most effective methods for fully mineralizing harmful organic pollutants has developed as photocatalysis, a nicely shaped offshoot of sophisticated oxidation processes. Its effectiveness and economic viability are further attested by the employment of low-cost resources including semiconductor materials, water, and light photons for the creation of O_2^- and OH^- (Mansournia & Ghaderi, 2017).

Photocatalytic activities are anticipated to be present in CuO@ZnO nanocomposites. The study of these nanocomposites as photocatalysts opens up new possibilities for pollution remediation in textile and dyes-related industries. The photochemical

oxidative reaction is a specific instance of photocatalysis in which a semiconductor surface is activated by UV light to produce free active oxygen species radicals such $^{\bullet}OH$, $^{\bullet}O_2^-$ and $^{\bullet}O_2H$. These species are thought to be the main players in the breakdown of organic pollutants. Under UV irradiation, the photo-induced electron-hole pairs in ZnO often split from one another. Positive holes (h^+) are left in the valence band as the electrons (e^-) transit from the valence band to the conduction band under the excitation by photons. Following the separation of electrons and holes, dissolved oxygen (O_2) adsorbed on the surface of the catalyst will react with photo-induced electrons to form superoxide anion radical ($^{\bullet}O_2^-$), and the holes (h^+) in the valence band will be positive enough to produce hydroxyl radicals from the adsorbed hydroxide ions and water molecules (Ahmed et al., 2010; Lathasree et al., 2004; Mansournia et al., 2016). In order to ascertain these phenomena, the green synthesis of CuO@ZnO nanocomposite is recommended.

1.7. Plant Description

Artemisia vulgaris, commonly known as mugwort and locally known as titepati in Nepal has a long history of its use in traditional systems of medicine in different parts of the world. This species is distributed worldwide (Weston et al., 2005) (Coopoosamy, 2015; Ivanescu et al., 2015; Sugiyama, 2015). The vegetative part of the plant with taxonomical classification is shown in figure 1.

Taxonomics classification

Kingdom: Plantae

Division: Magnoliophyta

Class: Magnoliopsida

Order: Asterales

Family: Asteraceae

Genus: *Artemisia*

Species: *vulgaris*

Common Name: Mugworth

Nepali Name: Titepati

Figure 1.1: *Artemisia vulgaris* plant (focusing leaves)

Artemisia vulgaris is a herb with 70-150 cm long, highly branched shrub, having pinatissect or bipinatissectas leaves with lanceolate or oblong segments, soft, white silver dorsally (Abiri et al., 2018). The leaves are sessile and pinnate, 5-20 cm long, dark green, and covered with thick white tomentose hairs on the underside. Mugwort rhizomes are light-brown, up to 1 cm in diameter, and can delve 7 to 18 cm into the soil. The blooms are virtually glabrous in appearance and reddish brown or yellowish in color. Oval shaped, measuring 3–4 mm length by 2 mm broad, are flower heads. Flowers are grouped in a cluster like an inflorescence (Barney & DiTommaso, 2003; Corrêa-Ferreira et al., 2014). The plant is bitter in taste and aromatic in nature, and the root is pungent and sweet.

Artemisia vulgaris is known to possess various types of secondary metabolites such as **falvonoids** like apigenin, chrysoeriol, diosmetin, eriodictyol, eupafolin, homoeriodictyol, isoquercitrin, isorhamnetin, jaceosidine, kaempferol 3,7-dimethyl ether, kaempferol, kaempferol-3-glucoside, kaempferol 3-rutinoside, kaempferol 7-glucoside, Luteolin, Luteolin 7-glucoside, Luteolin rutinoside, chrysosplenetin, artemetin, quercetin, quercetin 3,3'-dimethyl ether, quercetin 3,7,3'-trimethyl ether, quercetin 3,7-dimethyl ether, quercetin 3-galactoside, quercetin 3-glucoside, quercetin 7-glucoside, quercetin-3-malonylglucoside, quercetrin, rutin, tricine, vitexin), **phenolic acids** like 1,3-O-dicaffeoylquinic acid/1,4-Odicaff, 1,5-O-dicaffeoylquinic acid, 3,4-O-dicaffeoylquinic acid, 3,5-O-dicaffeoylquinic acid, 3-O-caffeoylquinic acid, 4,5-O-dicaffeoylquinic acid, 5-O-caffeoylquinic acid, 5-O-feruloylquinic acid, gallic acid, protocatechuic acid glucoside, **organic acids** like malic acid, quinic acid, trihydroxy-octadecenoic acid, tuberonic acid glucoside, **Sesquiterpene** like artemisinin, eudesmane dialcohol, new sesquiterpene 1, **Sesquiterpenic acid** like 3-oxoeudesma-1,4,11(13)-trien-7αH-12-oic acid, lα-hydroxyeudesma-2,4(15),11(13)-trien-5α,7αH-12-oic acid, **Sesquiterpene glucoside** like artemisinic acid glucoside isomer 1, artemisinic acid glucoside isomer 2, **Sesquiterpene lactone** like 1,2,3,4-diepoxy-11(13) eudesmen12,8-olide, vulgarin, yomogin, **Ignan glucoside** like tracheloside, **monoterpene** like dehydrovomifoliol, **monoamine neurotransmitter** like 5-HT,5- hydroxytryptamine, etc. (Lee et al., 1998, 1999**;** Nguyen et al., 2016**) (Supplimentary table-S2).**

Artemisia vulgaris has been used since ancient times for ethnopharmacological purposes such as antibacterial, antipyretic, anti-fertility, antitumor, and anti-malarial activities (Shanmuganathan et al., 2018).

1.8. Statement of problem

Environmental protection is one of the main topics of scientific societies, due to the rapid development of industry, and improved people's living standards. Modern civilization also brings the serious environmental pollution, especially water pollution. Water pollutions cause an adverse effect on human health and to the entire ecosystem. Especially organic pollutants are the most troublesome substances such as textile waste water and dyes. These types of pollutants are very difficult to be decomposed in the natural environment and cause serious problems. Different treatments were developed for water treatment such as filtration, oxidation, adsorption, and photocatalytic techniques. Many monometallic oxide nanomaterials such as ZnO, CuO, Fe_2O_3, SnO_2, TiO_2, etc. have been studied as photocatalysts but most of them have some obvious drawbacks as a photocatalyst, such as high recombination efficiency of photogenerated electrons and holes, the fact that it can only be excited by ultraviolet light with photon energy greater than the band-gap energy, and so on.

So to improve the photocatalytic behavior eco-friendly, convenient, and cost effective method has been used to prepare bimetallic CuO@ZnO nanocomposites by using leaf extract of *Artemisia vulgaris* which has nontoxic and natural capping agent that are easily available for everyone.

1.9. Objectives of the study

1.9.1. General Objectives

The general objective of this study is to carry out the green synthesis of CuO@ZnO nanocomposites using *Artemisia vulgaris* leaf extract and study of its photocatalytic activities on methylene blue.

1.9.2. Specific Objectives

The specific objectives of this study can be figured out as follows:

- Preparation of methanol extract of leaf and conduction of its phytochemical screening.
- Synthesis of CuO@ZnO nanocomposite using *Artemisia vulgaris* leaf extract as reducing and stabilizing agents by green method.
- Characterization of CuO@ZnO nanocomposite.
- Study of photocatalytic activities against Methylene Blue (MB).

CHAPTER 2
LITERATURE REVIEW

Various semiconductor nanomaterials, and metal oxides including TiO_2, ZnO, SnO_2, Fe_2O_3, etc. have been intensively studied as photocatalysts due to band matching, high photocatalytic activity performance, and stability against optical corrosion. In particular, ZnO has some distinct advantages over others such as direct band gap, simple customized structure, ease of crystallization, anisotropic growth, and higher exciton binding energy and electron mobility (Mansournia & Ghaderi, 2017).

However, ZnO has some obvious drawbacks as a photocatalyst, such as high recombination efficiency of photogenerated electrons and holes, the fact that it can only be excited by ultraviolet light with photon energy greater than the band-gap energy, and so on. The above-mentioned key difficulties must be resolved in order for ZnO materials to become viable photocatalysts (L. Xu et al., 2017).

Many efforts have been made to improve the photocatalytic effectiveness of ZnO nanostructures by changing their morphology, modifying ZnO with non-metal doping, and adding transition metals or forming composite (Qi et al., 2020).

CuO has received a lot of attention among these narrow bandgap semiconductors due to some advantages such as very stable physical and chemical properties and a bandgap of 1.5–2.1 eV. The nanocomposites formed by ZnO and CuO can use not only UV light but also visible light, making them suitable for use as photocatalysts with a visible light response (Das & Srivastava, 2018; L. Xu et al., 2017).

The nanocomposite demonstrated the highest photocatalytic performance when the molar ratio of ZnO: CuO was 2:1, which was generated using a microwave-assisted urea-nitrate combustion technique. This indicates that the amount of CuO in CuO/ZnO composites has a significant impact on photocatalytic activity. Although several CuO/ZnO nanocomposites have been made earlier using the hydrothermal approach, the procedures are rather complicated, and the influence of CuO contents on the photocatalytic performance of CuO/ZnO nanocomposites is rarely described (Sherly et al., 2015).

In a straightforward, economical, two-step hydrothermal process, Mansournia & Ghaderi, (2017) produced pure ZnO, CuO, and CuO@ZnO nanoparticles with success. The synthesized core shell CuO@ZnO has undergone rigorous morphological, crystallographic, structural, and photovoltaic characterization.

CuO@ZnO NC formation was verified by the XRD examination. Moreover, as formed ZnO and CuO have typical crystal sizes of roughly 26 and 21 nm, respectively. The breakdown of MB dye under UV irradiation was used to test the photocatalytic activity of CuO@ZnO. In comparison to using pure ZnO nanoparticles, a significant rise in the photocatalytic efficiency was seen when using 0.4 and 2% CuO@ZnO nanocomposites. After 90 minutes of UV exposure, the degradation of MB with 0.4 and 2% CuO@ZnO is measured to be 94% and 96%, respectively.

In the work by Yulizer, using *Theobroma cacao* seed bark extract, green synthesis of ZnO/CuO nanocomposites has been explored. Fluorescence spectrometer, UV-vis, DRS, FTIR, SEM, EDX, TEM, and XRD were used to identify the nanocomposites. ZnO/CuO nanocomposite measured 20–50 nm in size, according to TEM (Yulizar et al., 2018).

Plant extracts provided biomolecules that are safe, environmentally friendly, inexpensive, and readily available. As a result, biomolecules are a possible alternative to toxic compounds. Biomolecules discovered in extract serve an important function as reducing agents, stabilizing agents, or both of which have an impact on the properties and morphologies of the nanoparticles that result (M. Khan et al., 2018; Marslin et al., 2018).

According to Bordbar (Bordbar et al., 2018), in the absence of dangerous and toxic components, a CuO/ZnO nanocomposite was synthesized employing *Melissa afficinalis* L. leaf extract as a moderate, renewable, and non-toxic reducing agent and effective stabilizer. Nanocomposite has been characterized using SEM, EDX, TEM, and XRD. By using TEM analysis to examine the morphology of the CuO/ZnO nanocomposite, it was discovered that ZnO nanoparticles were joined to spherical, narrow-sized 10 to 20 nm CuO nanoparticles. Additionally, CuO/ZnO nanocomposite has demonstrated good catalytic activity in the aqueous degradation of 4-nitrophenol and Rhodamine B at room temperature.

CuO/ZnO is one of the metal oxide nanocomposites that researchers are most interested in because of its non-toxicity, cost-effectiveness, and availability. It has a high energy density as well as excellent electrical and piezoelectric capabilities. CuO/ZnO nanocomposites outperform pure ZnO and CuO nanostructures in terms of physicochemical properties. The development of a CuO/ZnO heterojunction also improves optical and electrical properties, which are thought to be useful in photocatalysis (Sakib, Masum, Hoinkis, Islam, Molla, et al., 2019).

Sakib, Masum, Hoinkis, Islam, & Molla, (2019) created CuO/ZnO composites by a straightforward mechanochemical combustion process. The estimated grains were determined to be 32.16 and 32.13 nm for ZnO and 5% CuO/ZnO, respectively, according to the XRD pattern, which revealed the crystal structure of wurtzite ZnO. The particles appear to be spheroid-shaped, according to SEM photographs. During sun irradiation, CuO/ZnO NCs demonstrated strong photocatalytic activity against MB dye. After 2 hours of sun exposure, the degradation value of MB with 5% CuO/ZnO is determined to be 98%. The photodegradation of MB is significantly influenced by the reactive species $\cdot O_2^-$ and OH^- radicals.

Without using a template, ZnO/CuO heterostructure hollow spheres were created. ZnO/CuO has a spherelike shape (4 nm) after coupling with CuO and is formed of nanoparticles (20 nm). The ZnO/CuO hollow spherical is an excellent photocatalyst and potentially destroys 97.8% of the RhB under natural sun irradiation within 100 min (Chen et al., 2020).

By utilizing the biomass filtrate of *Penicillium carylophilum*, the biosynthesis process has been expanded to allow for the manufacture of CuO/ZnO nanocomposites at various ratios. FTIR, XRD, TEM, SEM, EDX, and XPS were used to characterize all of the synthesized nanocomposites. The findings of XRD and TEM analysis showed that nanocomposites sizes ranged from 10 to 55 nm. MB was used to assess the produced nanocomposites' photocatalytic degradation effectiveness. By increasing the percentage of ZnO nanoparticles in the nanocomposite formulation, high photodegradation effectiveness was attained; 97% of organic MB dye was eliminated after 85 minutes of exposure using 20% CuO/ZnO nanocomposites (Fouda et al., 2020).

According to the research done by Thatikayala & Min, (2021), Biogenic nanocrystals (ZnO/CuO) were created from *Ginkgo bioloba* leaf extract and used as photocatalytic and antibacterial agents, according to research by Thatikayala et al., 2021. The creation of a crystalline ZnO/CuO nanocrystal was evident in the XRD patterns, and the globular shape in the HRTEM pictures suggested that the material was porous. After 60 minutes of UV exposure, the maximal photocatalytic degradation efficiency of MB dye with ZnO/CuO nanocrystal was 99%, which was much greater than the efficiency of the bare nanocrystals (75% for ZnO and 36% for CuO). Against Gram-negative bacteria, it also demonstrated strong antibacterial action.

Jery O. Aldeyemi's paper from 2022 claims that CuO-ZnO nanocomposites were effectively made utilizing phytochemical extract from *Dovyalis caffra* leaves. The characterization of synthesized nanocomposites was done using XRD, UV-VIS, SEM, FTIR, TEM, and EDX. The XRD examination verified the existence of hexagonal ZnO and monoclinic CuO, both of which were confirmed in the CuO-ZnO. When tested on MCF7 breast cancer cells, these newly created nanocomposites performed better than the corresponding metal oxides but only marginally better than conventional medications (Adeyemi et al., 2022).

For the fabrication of CuO-ZnO nanocomposites, (Bekru et al., 2022) employed an aqueous extract of *verbascum sinaiticum*. In order to investigate the crystallinity, optical characteristics, morphology, and other qualities of CuO-ZnO samples, XRD, spectroscopic, and microscopic techniques were utilized. For ZnO, CuO, and CuO-ZnO samples, the average crystallite sizes were 22, 14, and 18 nm, respectively. Also, the reduction and degradation of 4-nitrophenol and MB were examined for photocatalytic activity. The photocatalytic activity against MB dye in CuO-ZnO nanocomposites with 20% CuO was improved, with a rate constant of 0.017 min as opposed to 0.0027 min for ZnO nanoparticles.

In the work by Basavegowda et al., (2022), the bimetallic p-ZnO/n-CuO nanocomposite's photocatalytic activity against 4-nitroaniline and methyl orange was investigated using *Aegle marmelos* extract. By reducing 90 % of 4-nitroaniline in 20 minutes and degrading 96 % of Methyl orange in 10 minutes, it has been discovered that ZnO/CuO hetero-nanocomposite has high photocatalytic activity.

As per the study, the synthesis of CuO/ZnO nanocomposite using *Artemisia vulgaris* plant extract has not been reported yet.

As reported, aqueous extracts of *Artemisia vulgaris* leaves contain phytochemicals such as flavonoids, triterpenoids, glycosides, polyphenols, Saponins, and proteins (Thangjam et al., 2020) providing significant phytochemicals as a promising candidate for nanoparticle synthesis.

Considering the aforesaid studies into account, CuO@ZnO nanocomposites will be generated in this investigation utilizing an eco-friendly green approach using *Artemisia vulgaris* leaf extract as a reducing agent to achieve the enhanced photocatalytic activity.

CHAPTER 3

MATERIALS AND METHODS

3.1.Materials

3.1.1. Sample collection and study area

Artemisia vulgaris leaves were gathered from Sainamaina municipality ward No 11 (27°41′31.9″ N and 83°15′39.4″ E), Rupendehi, Nepal in September, 2022. The Amrit Campus in Thamel, Kathmandu, is part of the research area. It has a decent vibe and facilities for conducting experiments in order to complete the research. The leaf of *Artemisia vulgaris* has been used for this study.

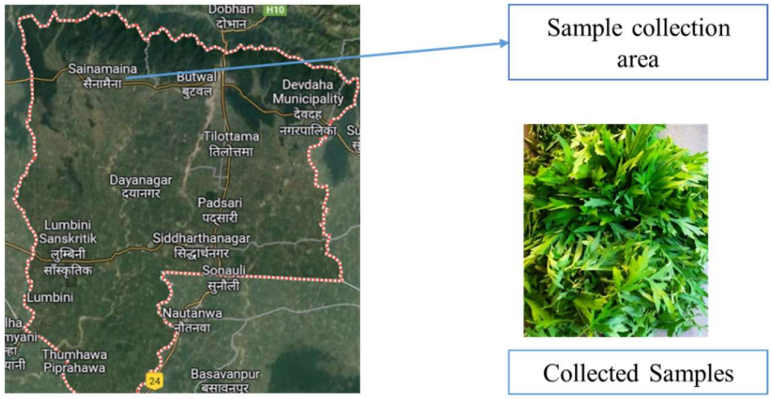

Figure 3.1: Sample collection area and collected samples

3.1.2. Equipment

Digital weighing balance, Spectrophotometer (Labrotonics-2802), Hot air Oven, Muffle Furnace, UV lamp, Sonicatar, Magnetic stirrer, Auto deluxe digital pH meter (Labrotonics-10, India), Dryer, Other glasswares.

3.1.3. Chemicals

All the chemicals used for this study were of analytical grade and were used as received without further purification.

a) Methanol (99.8 %, EMPARTA®)
b) Cupric nitrate trihydrate (95-103 %, Qualigens)
c) Zinc nitrate hexahydrate (96-103 %, Fisher Scientific)
d) Sodium hydroxide pellets (97 %, LOBA CHEMIE PVT.LTD)
e) Methylene blue (70 %, s.d. fine-chem limited)

3.2. Preparation Methods

3.2.1. Preparation of *Artemisia vulgaris* leaves extract

Artemisia vulgaris leaves were washed with distilled water, dried in the shade for 10-12 days, and then crushed to a fine powder using a pulverizing mill. The leaf extract was prepared by soaking 100 g of leaf powder in 750 mL methanol for 10 days and then filtered to obtain the extract.

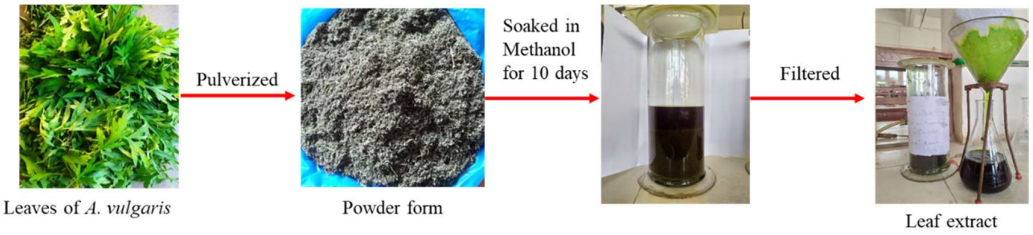

Scheme 4: Schematic representation of the leaf extract preparation.

3.2.2. Phytochemical Analysis

The bioactive substances in *Artemisia vulgaris* leaf extract can be identified with the use of phytochemical investigation. By examining the color reactions with certain reagents for particular bioactive compounds, the existence of the bioactive chemical was established.

3.2.3. Synthesis of CuO NPs

For the synthesis of CuO NPs slight modification was done in a previously reported protocol (Bekru et al., 2022). Firstly, 5.0 g of $Cu(NO_3)_2.3H_2O$ was taken and dissolved in 20 mL distilled water (DW) and heated at 70 °C under a magnetic stirrer. While it is being stirred, 25 mL of plant extract was slowly added to the solution and 2 mL (5 M) NaOH was added for adjusting the alkaline pH and then stirred for 60 min. Subsequently, the mixture was sonicated for 10 min. After that, the mixture was centrifuged, filtered, and washed with DW and ethanol. Thus obtained precipitate was dried at 80 °C for 12 hrs and crushed to make powder by a pestle. Eventually, the powder form was calcined for 3 hrs at 400 °C using a muffle furnace. The resulting product was pure CuO NPs.

3.2.4. Synthesis of ZnO NPs

For the synthesis of ZnO NPs slight modification was in a previously reported protocol (Bekru et al., 2022). Firstly, 5.0 g of $Zn(NO_3)_2.6H_2O$ was taken and dissolved in 20 mL DW and heated at 70 °C under a magnetic stirrer. While it is being stirred, 25 mL of plant extract was slowly added to the solution and 2 mL (5 M)

NaOH was added for adjusting the alkaline pH and then stirred for 60 min. Subsequently, the mixture was sonicated for 10 min. After that, the mixture was centrifuged, filtered and washed with DW and ethanol. Thus obtained precipitate was dried at 80 °C for 12 hrs and crushed to make powder by a pestle. Eventually, the powder form was calcined for 3 hrs at 400 °C using a muffle furnace. The resulting product was pure ZnO NPs.

3.2.5. Synthesis of CuO@ZnO nanocomposites

Typically, 2.5 g of $Cu(NO_3)_2.3H_2O$ and 2.5 g of $Zn(NO_3)_2.6H_2O$ were taken and dissolved in 20 mL DW and heated at 70 °C under a magnetic stirrer. While it is being stirred, 25 mL of plant extract was slowly added to the solution and 2 mL (5 M) NaOH was added for adjusting the alkaline pH and then stirred for 60 min. Subsequently, the mixture was sonicated for 10 min. After that, the mixture was centrifuged, filtered and washed with DW and ethanol, thus obtained precipitate was dried at 80 °C for 12 hrs and crushed to made powder by a pestle. Eventually, the powder form was calcined for 3 hrs at 400 °C using a muffle furnace. The resulting product was 50 % CuO@ZnO nanocomposite.Similarly, other samples with CuO content of 2, 5 and 25 % by wt % were prepared using $(NO_3)_2.3H_2O$ (0.1 g, 0.25 g and 1.25 g) and Zn $(NO_3)_2.6H_2O$ (4.9 g, 4.75 g, and 3.75 g), respectively.

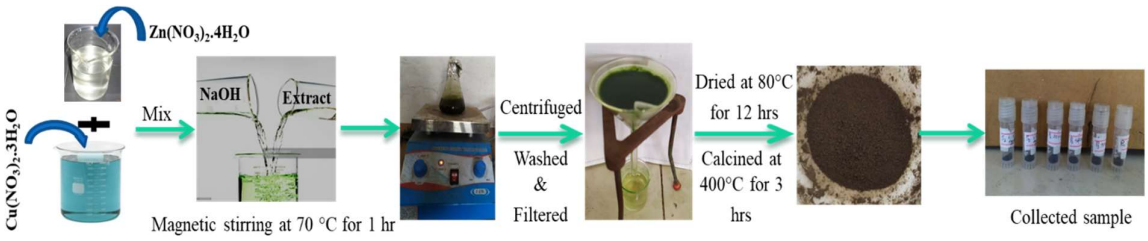

Scheme 5: Schematic design for the synthesis of CuO@ZnO NCs.

3.3. Physicochemical Characterization

Structural and morphological characterizations were carried out using different instruments, such as UV spectroscopy, FT-IR, XRD, EDX, and FESEM. Photocatalytic efficacy of as-synthesized composite materials was performed using Methylene Blue solution as a model compound. The phytochemical test was based on the chemical test method where visual changes were noted.

UV-visible spectroscopy was used to determine the formation of CuO NPs, ZnO NPs, CuO@ZnO nanocomposites. UV- visible spectrometer (Labrotonics, model LT2802)

having double beam wavelength from 200 to 800 nm was run through the sample solution (at a concentration of 1 mg/10 mL distilled water) using a cuvette and absorbance was observed. It was carried out in the Department of Chemistry, Amrit Campus, Kathmandu.

Fourier Transform Infrared (FTIR) Spectroscopy was used to identify the functional group associated with the sample as a stabilizing and reducing agent. The FTIR spectra were recorded with an FTIR spectrometer (PerkinElmer 10.6.2) at the cut off range 400-4000 cm^{-1} with scan interval 4 cm^{-1}. It was also carried out in the Department of Chemistry, Amrit Campus, Kathmandu.

The crystallinity and crystal phase of the obtained materials were probed by an X-ray diffraction (XRD) instrument (Cu Kα (λ = 1.5406 Å) radiation on a Rigaku diffractometer, JNCASR, Bengaluru, India). The crystal structure of the synthesized CuO, ZnO, and CuO@ZnO was examined by XRD. The surface morphology of thecomposite was studied using Field emission scanning electron microscopy (FESEM, Hitachi, Tokyo, Japan) equipped with energy dispersive x-ray spectroscopy (EDX).

The whole experiment was carried out based on the following framework.

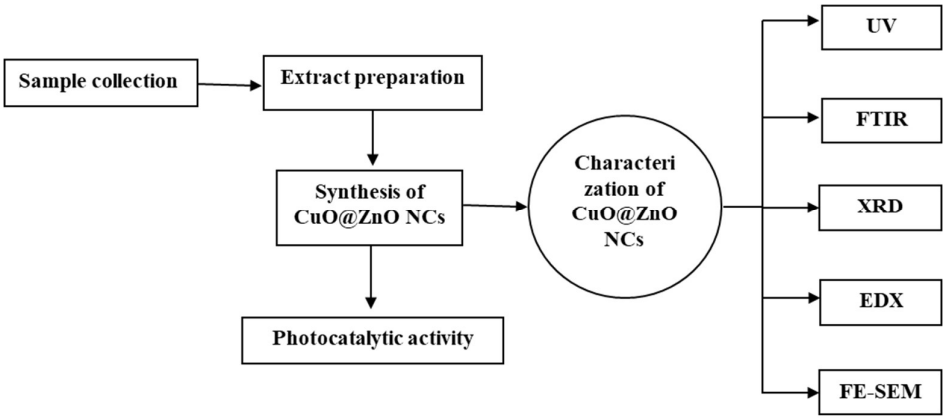

Scheme 6: Systematic organization of the study work

3.3.1. Photocatalytic activity

Photocatalytic activities of the CuO/ZnO NCs were investigated by exposing 50 mL of 5 ppm methylene blue (MB) containing 30 mg of CuO/ZnO nanocomposite with constant magnetic stirring in a glass beaker under UV light (a series of six Philips UV lamps 15 W having a center wavelength of 254 nm positioned at 20 cm a distant over the suspension surface) source. In order to ensure adsorption/desorption equilibrium, the solution was stirred for 30 min in dark, prior to the irradiation. The absorbance of

the irradiated sample solution was recorded using UV-double beam spectrophotometer in each 15 min interval. The experimental conditions for all set of experiments are tabulated in table 2. The percentage of photocatalytic degradation (D %) was evaluated by using equation (1).

$$D\ \% = \frac{C_0 - C_t}{C_0} \times 100 \qquad \ldots (1)$$

Where, C_o and C_t are concentration at time 0 and t. k is rate constant

Table No.1: Experimental Conditions

Methylene Blue	50 mL, 5 ppm
Photocatalyst	CuO@ZnO composites, 30 mg for 50 mL MB (5 ppm)
Temperature	25 ˚C
pH	Natural
Light source	UV light
Irradiation time	0- 90 min

CHAPTER 4

RESULTS AND DISCUSSION

4.1. Phytochemical analysis

Methanol extract from leaves of *Artemisia vulgaris* was successfully carried out. Phytochemical analysis of methanol extract of leaf of *Artemisia vulgaris* was done according to the standard protocol (*Supplementary Table S2*).

The results are tabulated below;

Alkaloids	Absent
Flavonoids	Present
Saponins	Present
Terpenoids	Present
Quionens	Present
polyphenols	Present
Proteins	Present
Glycosides	Present

As per the study, alkaloids was found to be absent in the leaves extract, whereas the bioactive compounds like Flavonoids, Saponins, Terpenoids, Quionens, Polyphenols, Proteins, and Glycosides were found to be present. These bioactive phytoconstituents were believed to act as reducing as well as stabilizing agents for the synthesis of nanomaterials. While, study performed by Thangjam et al., (2020) showed that, leaves extract of *Artemisia vulgaris* contained phytochemicals such as flavonoids, triterpenoids, glycosides, polyphenols, Saponins, and proteins (Thangjam et al., 2020). Our finding is in good agreement with the finding.

4.2. UV-Vis Spectroscopy

Finding of UV-vis spectroscopic characterizations are shown in figure 4.1. It is found that all of the produced materials, including ZnO, CuO, and CuO@ZnO, substantially absorb in the UV area at 325 nm. Nevertheless, the CuO@ZnO nanocomposites also exhibited shoulder peaks in UV-vis spectra around 430 nm. The red shift in the UV-VIS absorbance of the composite could be associated with the agglomeration of particles into relatively larger sizes or may be due to the some sort of defeats.

In comparison to ZnO, the CuO, and CuO@ZnO showed a broad peak. The absorption peaks get widened with the percentage increase of CuO. It has been

reported that the presence of CuO causes larger adsorption in the visible region (Bekru et al., 2022).

Likewise, our finding, Kalia et al., (2021) found that the UV absorbance maxima of the CuO and ZnO nanoparticles were at 320 nm and 330 nm, respectively. ZnO nanoparticles and CuO-ZnO nanocomposites were discovered to have UV absorption maxima at 374 nm (Bekru et al., 2022). Bimetallic Cu-Zn nanoparticles were synthesized by Merugu et al., (2021), and their UV-visible spectra also revealed peaks at 338 nm. Similarly, Minal & Prakash, (2016) determined that the wavelength of Cu-Zn nanoparticles' UV-visible spectrum is 401 nm. The variation in the UV-VIS absorption of copper oxide/zinc oxide nanocomposites could be associated with the different particle size and attachment/doping of different phytochemical constituents onto the particles.

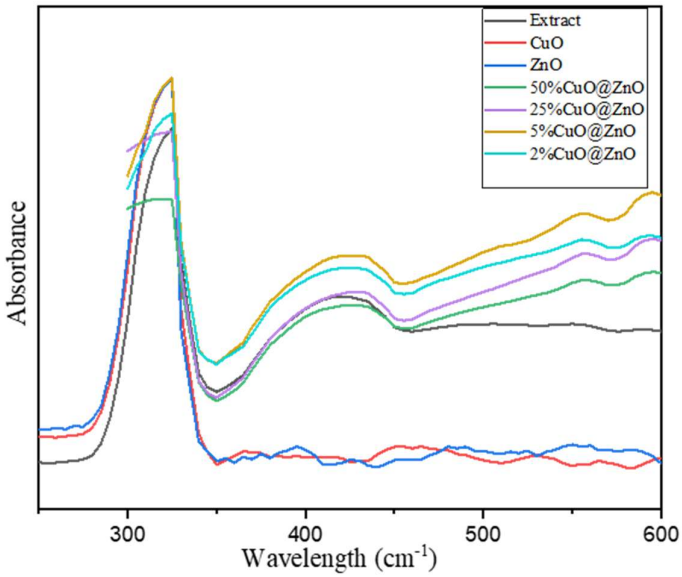

Figure 4.1: UV-visible spectra of CuO, ZnO, and CuO@ZnO nanocomposites

4.3. FTIR

The functional groups present in as-synthesized products were investigated using FTIR Spectroscopy. The FTIR spectra of plant extract and synthesized nanostructure were shown in figure 4.2. In the spectra of leaves extract, the board spectrum at 3323 cm^{-1} was due to the O-H bond stretching. Similarly, the C–H stretching of alkane has resulted in a band at 2945 cm^{-1} and 2833 cm^{-1}. C=O stretching of alkene, cyclic

alkene, imine, oxime, etc. are resulted in a band at 1656 cm^{-1}. The C–H bending of alkane give rise to band at 1449 cm^{-1} and 1413 cm^{-1}. An absorption peak at 1114 cm^{-1} was ascribed to C-N stretching, and band at 1022 cm^{-1} was attributed to of ester and tertiary alcohol. These peaks assigned were carried out accordance to the Spectrometric identification of organic compounds (Silverstein & Bassler, 1962). The functionalities present in the methanolic extract of leaves of *Artemisia vulgaris* were found to be well-indexed with some previously published report (Karki et al., 2023). Hereafter, in the spectra of ZnO NPs, O-H bond stretching of the phenolic group was observed at 3450 and 3369 cm^{-1}, likewise, the peaks as 1645 cm^{-1} and 1370 cm^{-1} attributed as C=O stretching and stretching modes of nitrate anions, respectively.

On the same way, in the spectra of CuO NPs, the peak at 3451 cm^{-1} assigned as O-H stretching, peaks at 2924 and 2818 cm^{-1} attributed as C-H stretching, 1745 cm^{-1} as C=O stretching and 1465 cm^{-1} as C-H bending (Karki et al., 2023; Mansournia & Ghaderi, 2017; Silverstein & Bassler, 1962). Furthermore, in all spectra of synthesized NPs and NCs, the bands appeared in the range of 400- 650 cm^{-1} were assigned as metal-oxygen (M-O) stretching vibrations which was well indexed to some reports (Mansournia & Ghaderi, 2017).

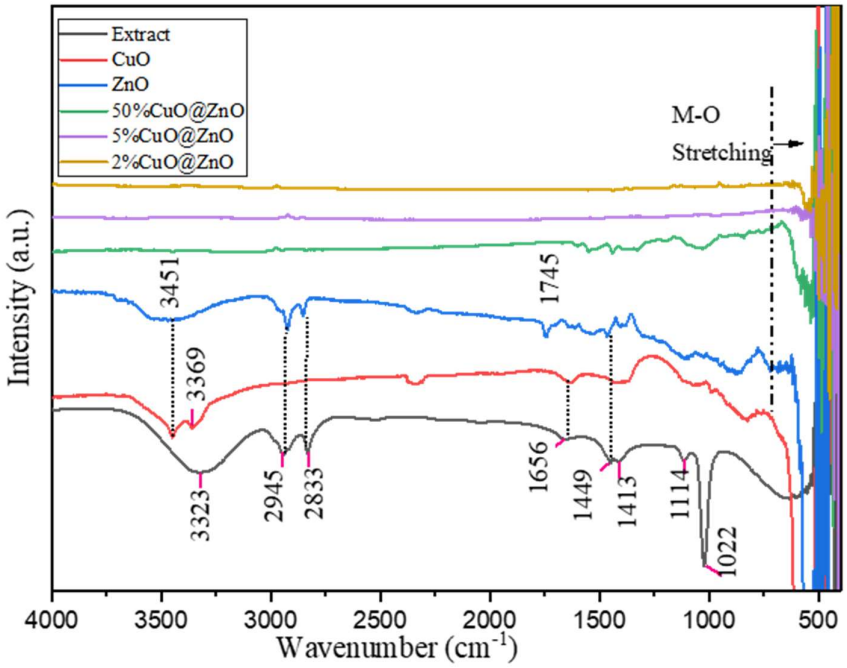

Figure 4.2: FTIR spectra of as-synthesized CuO, ZnO, CuO@ZnO, and Plant Extract

4.4. XRD

The crystallinity of the synthesized materials was examined by using XRD. The comparison of the XRD patterns of the as synthesized nanostructure is shown in figure 4.3. The XRD pattern of zinc oxide nanostructure was appeared at 2θ values of 31.7˚, 34.38˚, 36.2˚, 47.52˚, 56.52˚,62.8˚ and 67.9˚ which were well indexed to the (100), (002), (101), (102), (110), (103) and (112) plane of hexagonal ZnO, respectively, with JCPDS card no: 05-0664, space group: $p6_3/mc$, cell constant: a=b=3.249 Å and c=5.205 Å (G. Li et al., 2015). Similarly, the XRD patterns of copper oxide nanostructure appeared at 2θ values of 32.62˚, 35.70˚, 38.88˚, 48.92˚, 53.34˚, 58.40˚, 61.7˚, 66.46˚ and 68.16˚ which were in good agreement to (110), (11-1), (111), (20-2), (020), (202), (11-3), (31-1), and (220) plane of monoclinic CuO, respectively, with JCPDS card no: 41-05682, space group: C_{12}/C_1, cell constant: a=4.6949 Å , b=3.4382 Å , and c=5.187 Å (Smura et al., 2011). The diffraction peaks of CuO@ZnO at 2θ values were matched with the diffraction peak of ZnO and CuO, confirming the formation of CuO@ZnO NCs.

These synthetic ZnO and CuO nanostructures' XRD patterns showed no extra peaks, indicating that the materials were single-phase and hence extremely pure. Additionally, the Debye-Scherrer equation (3) was used to compute the average crystallite size of the produced Zinc oxide and Copper oxide nanoparticles.

$$D=\frac{K\lambda}{\beta\cos\theta} \quad \ldots (3)$$

Where,

D= Crystallite size of materials

λ= Wavelength of Cu Kα radiation (0.15406 nm)

θ = Bragg's angle

β = Corrected half width of the diffraction peak (in radian)

K= Shape factor which usually equals to 0.94

Furthermore, the average crystallite size of as-synthesized CuO, ZnO, and CuO@ZnO nanostructures were found at around 17.24 nm and 20.74 nm, and 19-24 nm, respectively.

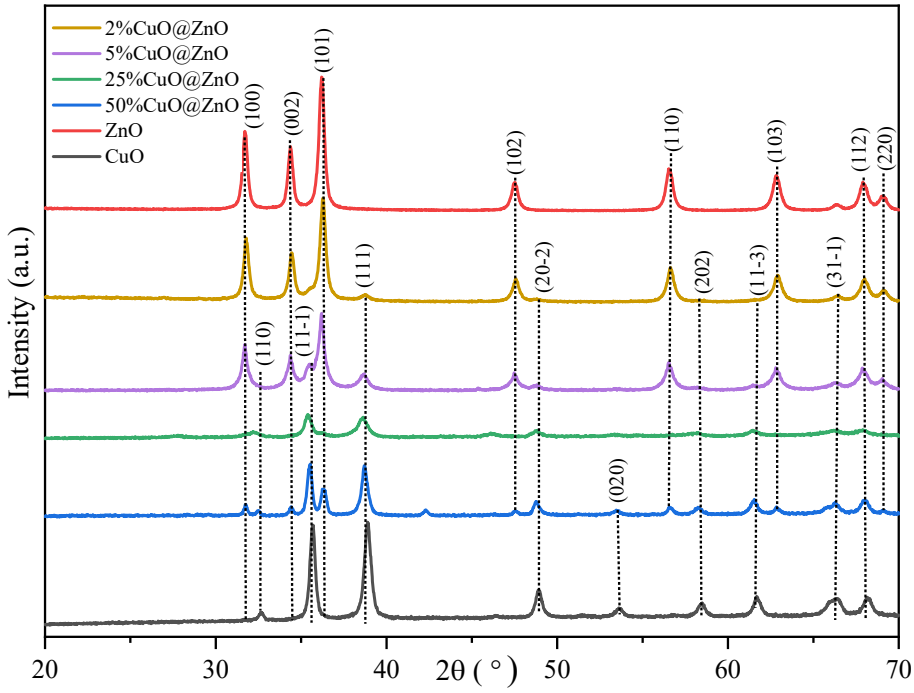

Figure 4.3: XRD patterns of the as-synthesized samples: CuO, ZnO, 50%CuO@ZnO, 25%CuO@ZnO, 5%CuO@ZnO, and 2%CuO@ZnO.

As seen in the figure 4.3, the intensity of ZnO peaks were significantly decreased with an increasing percentage of CuO in the CuO@ZnO nanocomposite structures. Hence, among the nanocomposites, the intensity of ZnO peaks were maximum at 2%CuO@ZnO nanocomposite whereas minimum at 50%CuO@ZnO. Meanwhile, the intensity of CuO peaks increased with increasing percentage of CuO in the CuO@ZnO nanocomposite structures, and the intensity of the CuO peaks were found to be maximum at 50%CuO@ZnO whereas minimum at 2%CuO@ZnO nanocompostes. However, in lower percentages of copper oxide, XRD technique is not able to verify the presence of CuO, due to the small amount of CuO coated on ZnO i.e. CuO peaks were found to be in a negligible amount at 2% CuO@ZnO NCs. These findings are in good agreement with other's report presented by (Bekru et al., 2022; Fouda et al., 2020; Mansournia & Ghaderi, 2017; Sakib, Masum, Hoinkis, Islam, & Molla, 2019; Yulizar et al., 2018).

4.5. FE-SEM

The surface morphology of as-synthesized CuO@ZnO nanocomposite is shown in figure 4.4. The image shows the particles of nanosize dimension. As there is no significant aggregation of composite nanoparticles, the leaf extract of *Artemisia vulgaris* serves as a good capping agent.

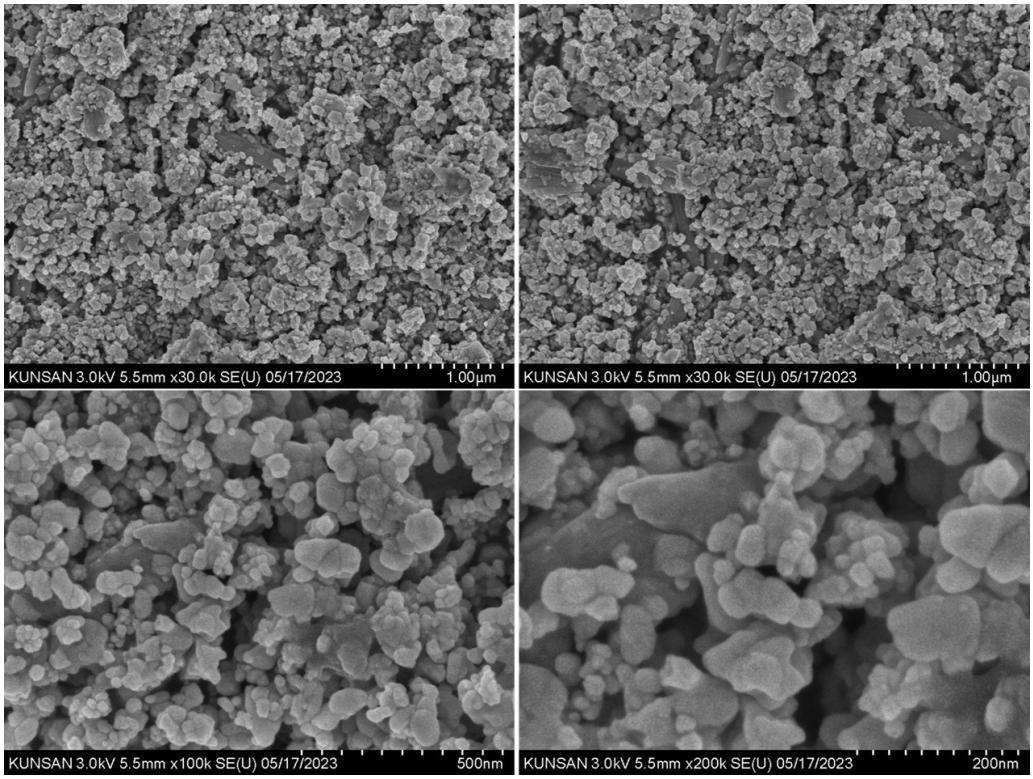

Figure 4.4**:** FE-SEM of 2% CuO@ZnO nanocomposites at different magnifications.

4.6. EDX spectroscopy

Energy dispersive X-ray spectroscopy (EDX) was employed to further demonstrate the production of CuO@ZnO nanocomposites. This method showed that the elements zinc, copper, and oxygen were present in every synthetic NCs. For instance, figure 4.5 shows the EDX spectrum of the nanocomposites with the smallest quantity of copper (2% CuO@ZnO).

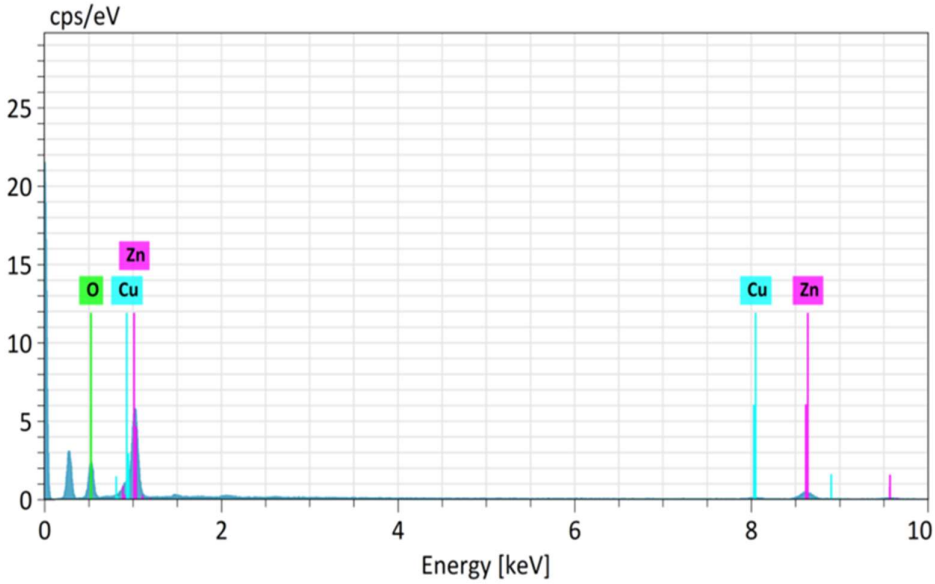

Figure 4.5: EDX spectrum of a typical 2 %CuO@ZnO NCs

Element	At. No.	Mass (%)	Mass Norm. (%)	Atom (%)	Abs. error (%) [3 sigma]
O	8	22.13	27.67	60.91	9.98
Cu	29	6.92	8.65	4.79	1.38
Zn	30	50.94	63.68	34.30	6.13
		79.99	100.00	100.00	

4.7. Photocatalytic activity

4.7.1. Wavelength scanning

The absorbance spectra of MB solution containing CuO, ZnO, and various ratios of CuO@ZnO nanocomposites are shown in figure 4.6 (a-f). A prominent peak at 665 nm of pure MB solution was recorded. Pure MB solution with the addition of different catalysts was subjected for 90 minutes to UV light irradiation. A subsequent decrease in the absorbance of the solution in each successive interval was observed. As compared to pure ZnO and CuO nanoparticles, the absorption band of CuO@ZnO nanocomposites was observed to be more reduced. The absorption spectra were found to be much lower in CuO@ZnO as the quantity of CuO dropped. Research showed that MB degraded in as-synthesized nanocomposites when exposed to UV exposure.

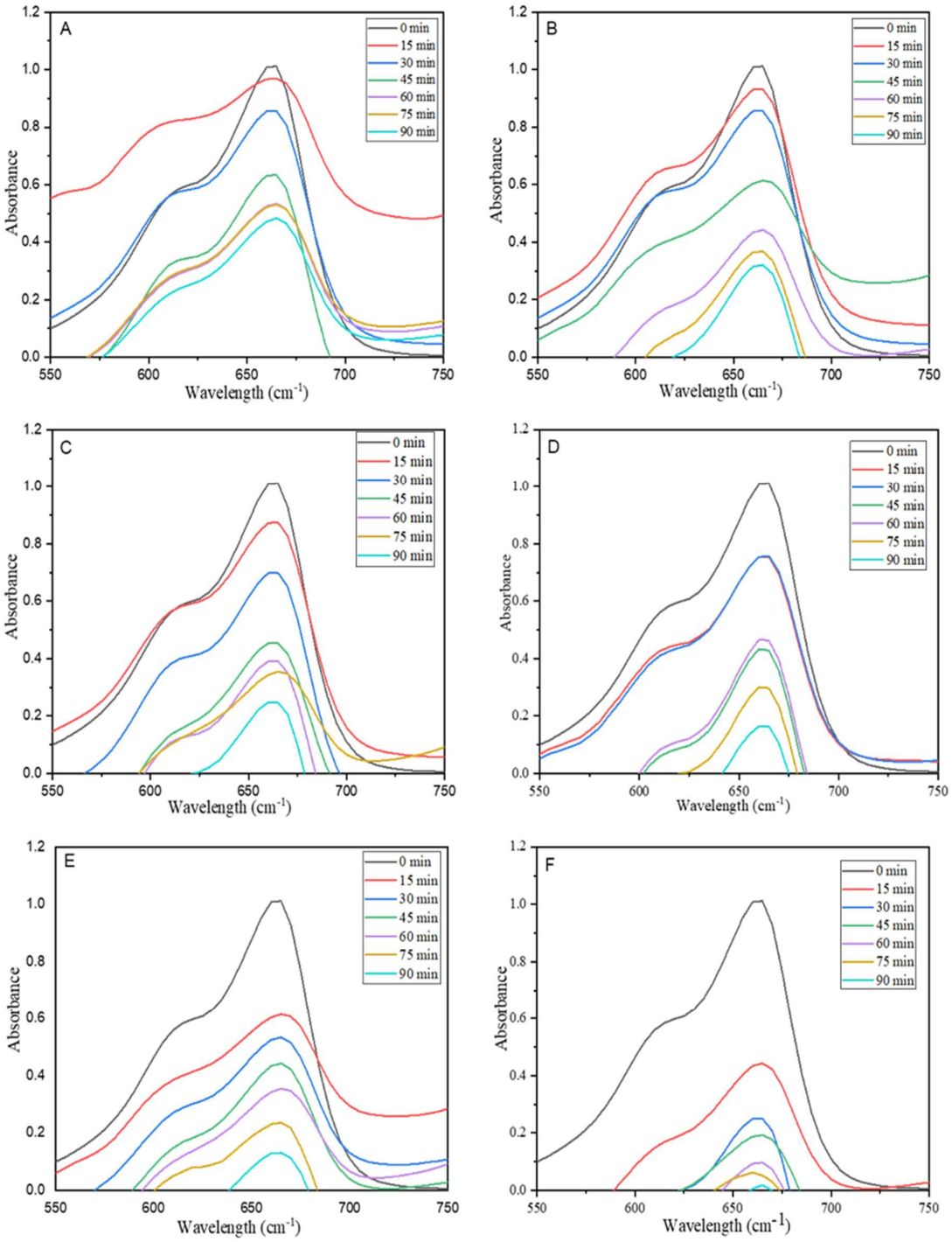

Figure 4.6: Photocatalytic removal of MB using (A) CuO, (B) ZnO, (C) 50% CuO@ZnO, (D) 25% CuO@ZnO, (E) 5% CuO@ZnO, and (F) 2% CuO@ZnO

4.7.2. Photocatalytic degradation and degradation efficiency

For the photodegradation of MB in the presence of UV light, CuO, ZnO, and different ratios of CuO@ZnO nanocomposites were utilized to assess the photocatalytic performance. Figure 4.7 illustrates the role played by copper concentration in the photodegradation of MB. The deterioration rate increased as the quantity of copper decreased, reaching its peak at 2% CuO@ZnO.

Figure 4.8 compares the degradation efficiency of all the green synthesized catalysts at 90 min, evaluated by using the equation 1.

The order of degradation rate is as follows: CuO < ZnO < 50%CuO@ZnO < 25% CuO@ZnO < 5% CuO@ZnO < 2% CuO@ZnO.

The degradation efficiency of CuO, ZnO, 50%CuO@ZnO, 25%CuO@ZnO, 5%CuO@ZnO, and 2%CuO@ZnO were found to be 52%, 68%, 75%, 83%, 87%, and 98% respectively.

In comparison to ZnO NPs alone, all CuO@ZnO samples performed better. With a 98% degradation efficiency, 2% CuO@ZnO displayed the highest photocatalytic activity. According to earlier research, the reduced performance of CuO@ZnO with higher CuO concentration beyond the optimal value may be due to increased aggregation of CuO that obscures surface photoactive sites or increased e/h recombination rates (Babu et al., 2019).

The transfer of e^- and h^+ from CuO to ZnO, is energetically prohibited at higher CuO coating levels (50%CuO@ZnO), where the majority of photons may be directly absorbed by CuO. Thus, more CuO coating results in a reduction in the amount of superoxide anion radical production ($^{\bullet}O_2^-$) and the catalyst's degradative activity. Whereas, with lower amount of CuO coating, NCs have significant potential to generate superoxide and hydroxyl radicals due to the potential of excited electron transfer from conduction band of thin layer CuO to that of ZnO, and transfer of holes from Valence band of ZnO to that of CuO, which is also an energetically permitted process. Moreover, in moderate CuO coated NCs the production and reduction of superoxide radicals and hydroxyl radicals both are impacted by the energetically preferred process of transfer of electrons and holes pairs (Chang et al., 2013; Khanchandani et al., 2012; Qamar et al., 2015; S. Xu et al., 2010). Hence, it was found that the activity of composite increased with decreased in amount of copper content.

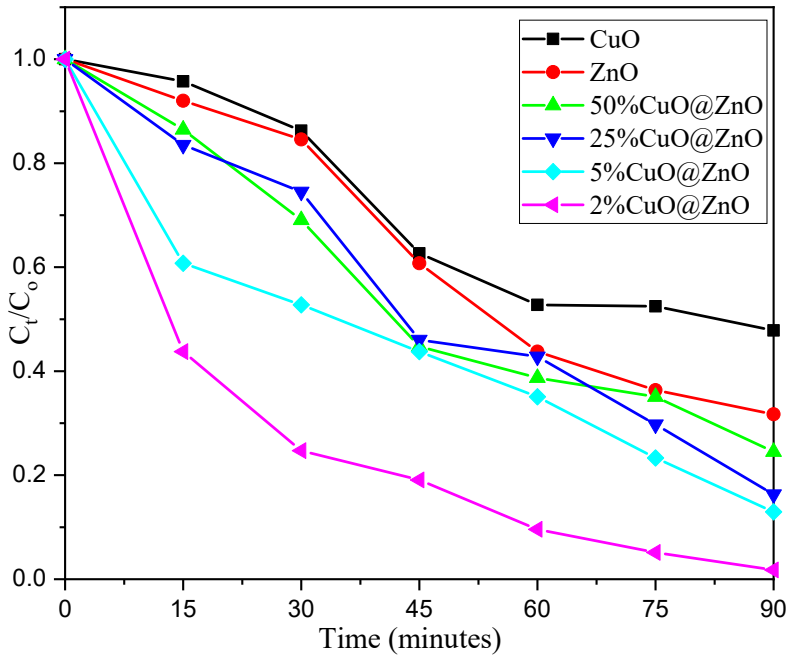

Figure 4.7. Photocatalytic degradation of MB solution under UV light in the presence of different samples versus irradiation time

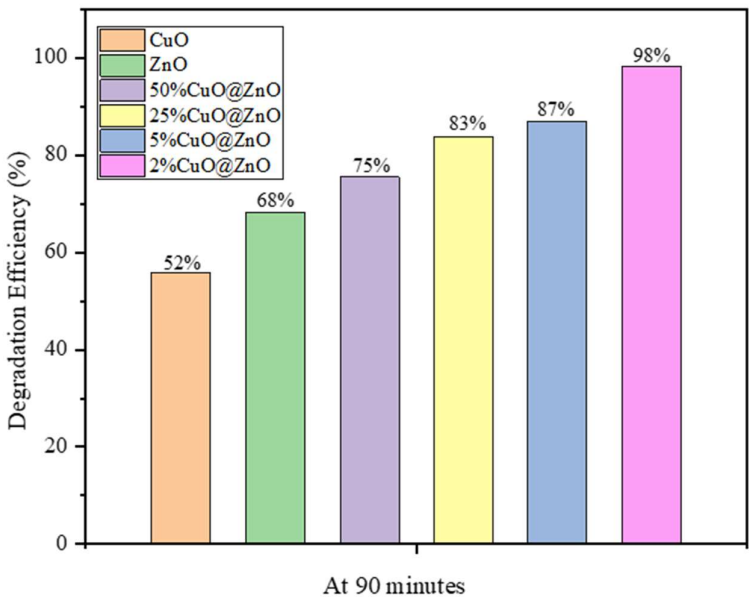

Figure 4.8. Degradation efficiency at the time of 90 minutes.

Table No.3: The comparison of photocatalytic efficiency of CuO@ZnO nanocomposite against organic pollutants reported in some papers;

Methods of synthesis	Pollutants	Amount of photocatalyst	Conc. Of pollutant	Light source	Time	D%	Reference
Mechanochemical combustion	MB	20 mg, 5%CuO/ZnO	5 ppm	Sunlight	2 hrs	98%	Sakib, & Molla, 2019
MW assisted using GH leaves	MB	20 mg, 20%CuO/ZnO	10 ppm	Visible light	105 min	82%	Bekru et al., 2022
Green synthesis using *penicillium corylophillium*	MB	40 mg, $CuO/ZnO_{20/80}$	10 ppm	Visible light	85 min	97%	Fouda et al., 2020
Noval hydrothermal	MB	20 mg, 2%CuO@ZnO	5 ppm	UV light	90 min	96%	Mansournia & Ghaderi, 2017
Green method using *Melissa officinalis* aq. leaves extract	RhB 4-NP	5 mg	2.5×10^{-3} M	Sunlight	5th cycle	100 %	Bordbar et al., 2018
Hydrothermal	RhB	1.0 g	1×10^{-5} mol L	Natural sunlight	100 min	97.8 %	Chen et al., 2020
Green synthesis using *Aegle marmelos* leaf extarct	4-nitroaniline MO	0.2 mg	0.025 mM	Sunlight	20 min 10 min	90% 96%	Basavegowda et al., 2022
One step bio combustion using Ginko leaf extract	MO MB	0.04 mg, 0.2%CuO/ZnO	10 ppm	UV light	60 min	83% 99%	Thatikayala & Min, 2021
One step hydrothermal	MB	20 mg, 2:1Zn;Cu CuO/ZnO	6 mg/L	Xe lamp	120 min	82%	Xu et al., 2017
Hydrothermal	MB	6%ZnO-24%CuO	1.5 mg/ 200 mL water	UV light	120 min	89%	Taufique et al., 2018
Photodeposition method	MO	50 mg	10 mg/L	UV lamp	120 min	93%	Wang et al., 2011
Green method using *A.vulgaris* leaf extract	**MB**	**30 mg**	**5 ppm**	**UV lamp**	**90 min**	**98%**	**This paper**

4.7.3. Degradation mechanism

CuO@ZnO has a higher photocatalytic effectiveness than pure ZnO due to the interfacial charge separation and strong charge separation. Using a CuO@ZnO nanocomposite, the predicted process for improved dye photodegradation is put forth in figure.In this study, the green technique employing *Artemisia vulgaris* leaf extract may have created a heterojunction between the surfaces of ZnO and CuO semiconductors and triggered the photodegradation of dyes, which was a key component of the photocatalysis mechanism.

The schematic diagram of the CuO@ZnO heterojunction's excitation and transfer of electrons and holes under UV light irradiation is shown in Fig.4.9. The heterojunction created by CuO and ZnO helped to separate the photogenerated carriers (Chabri et al., 2016).

ZnO and CuO were found to have valence band potentials of 2.42 and 1.43 ev, respectively, and conduction band potentials of -0.14 ev and -0.38 ev, respectively(Thatikayala & Min, 2021). Since, CuO is a narrow band-gap semiconductor, the CuO@ZnO hollow sphere can produce photogenerated electrons and holes after irradiation by UV light. The location of conduction and valence bands of CuO is higher than those of ZnO's, which is thermodynamically beneficial for the transfer of charge carriers created by light (Sherly et al., 2015). The photogenerated electrons will move from the conduction band of CuO to that of ZnO when exposed to UV radiation, whereas the photogenerated holes will move from the valence band of ZnO to that of CuO. Thus, due to the buildup of charge carriers like e^- in ZnO's conduction band and h^+ in CuO's valence band, the oxidation and reduction mechanisms over the surfaces of ZnO and CuO, respectively, result in the generation of superoxide ($^{\bullet}O_2^-$) and hydroxyl ($^{\bullet}OH$) radicals with the interaction of dissolved oxygen (O_2) and H_2O, respectively. Last but not least, the dye (MB) molecules engage in interactions with photogenerated radicals and fragment into more basic compounds. The dye molecules engage with photogenerated radicals and break down into smaller, less harmful organic compounds, which are then further transformed into CO_2 and water molecules, respectively (Karnati et al., 2018).

Here we proposed the following possible degradation mechanism of MB with CuO@ZnO in the presence of UV light.

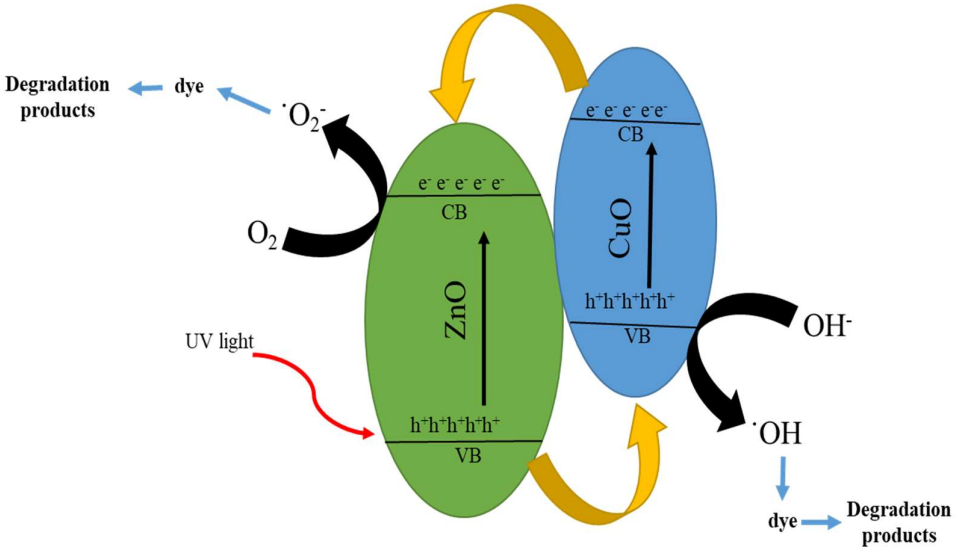

Figure 4.9. Possible degradation mechanism of CuO@ZnO photocatalyst under UV light.

$$CuO@ZnO + UV\ light \longrightarrow CuO@ZnO\ (e^-_{CB} + h^+_{VB})$$

$$CuO@ZnO\ (e^-_{CB} + h^+_{VB}) \longrightarrow CuO\ (h^+_{VB}) + ZnO\ (e^-_{CB})$$

$$e^-_{CB} + O_2 \longrightarrow \cdot O_2^-$$

$$h^+_{VB} + H_2O \longrightarrow \cdot OH$$

$$\cdot O_2^- + MB \longrightarrow degraded\ products$$

$$\cdot OH + MB \longrightarrow degraded\ products$$

CHAPTER 5

CONCLUSION

Highly efficient CuO@ZnO NCs have been successfully synthesized using leaves extract of *Artemisia vulgaris* through cost-effective, environmentally friendly, non-hazards green method. Thus synthesized CuO@ZnO NCs have been found to show significant photocatalytic activities. Thus synthesized NCs were used for the catalytic photodegradation of methylene blue (MB) and found to shown significant photocatalytic activities. The degradation efficiency of CuO, ZnO, 50% CuO@ZnO, 25% CuO@ZnO, 5% CuO@ZnO, and 2% CuO@ZnO were found to be 52 %, 68 %, 75 %, 83 %, 87 %, and 98 % respectively. Since, the nanocomposite with the lower concentration of CuO coated on ZnO exhibited effective separation and transport of photo-induced electro-hole pairs than that of pure ZnO, the composite with the lower amount of CuO coated on ZnO nanostructures enhanced the yield of photocatalytic degradation as compared to the higher amount of CuO coated on ZnO nanostructures. Therefore, it was found that, CuO@ZnO nanocomposites have potential to degrade MB as organic dye, and can be used for the wastewater treatment.

REFERENCES

Abiri, R., Silva, A. L. M., de Mesquita, L. S. S., de Mesquita, J. W. C., Atabaki, N., de Almeida Jr, E. B., Shaharuddin, N. A., & Malik, S. (2018). Towards a better understanding of Artemisia vulgaris: Botany, phytochemistry, pharmacological and biotechnological potential. *Food Research International*, *109*, 403–415.

Adeyemi, J. O., Onwudiwe, D. C., & Oyedeji, A. O. (2022). Biogenic Synthesis of CuO, ZnO, and CuO–ZnO Nanoparticles Using Leaf Extracts of Dovyalis caffra and Their Biological Properties. *Molecules*, *27*(10), 3206.

Ahmad, S., Munir, S., Zeb, N., Ullah, A., Khan, B., Ali, J., Bilal, M., Omer, M., Alamzeb, M., & Salman, S. M. (2019). Green nanotechnology: A review on green synthesis of silver nanoparticles—An ecofriendly approach. *International Journal of Nanomedicine*, 5087–5107.

Ahmed, S., Rasul, M. G., Martens, W. N., Brown, R., & Hashib, M. A. (2010). Heterogeneous photocatalytic degradation of phenols in wastewater: A review on current status and developments. *Desalination*, *261*(1–2), 3–18.

Alivisatos, A. P., Johnsson, K. P., Peng, X., Wilson, T. E., Loweth, C. J., Bruchez Jr, M. P., & Schultz, P. G. (1996). Organization of'nanocrystal molecules' using DNA. *Nature*, *382*(6592), 609–611.

Anastas, P. T., & Warner, J. C. (1998). Principles of green chemistry. *Green Chemistry: Theory and Practice*, *29*.

Aritonang, H. F., Koleangan, H., & Wuntu, A. D. (2019). Synthesis of silver nanoparticles using aqueous extract of medicinal plants'(Impatiens balsamina and Lantana camara) fresh leaves and analysis of antimicrobial activity. *International Journal of Microbiology*, *2019*.

Babu, S. G., Karthik, P., John, M. C., Lakhera, S. K., Ashokkumar, M., Khim, J., & Neppolian, B. (2019). Synergistic effect of sono-photocatalytic process for the degradation of organic pollutants using CuO-TiO2/rGO. *Ultrasonics Sonochemistry*, *50*, 218–223. https://doi.org/10.1016/j.ultsonch.2018.09.021

Barney, J. N., & DiTommaso, A. (2003). The biology of Canadian weeds. 118. Artemisia vulgaris L. Canadian Journal of Plant Science, 83(1), 205–215.

Basavegowda, N., Somu, P., Shabbirahmed, A. M., Gomez, L. A., & Thathapudi, J. J. (2022). Bimetallic p-ZnO/n-CuO nanocomposite synthesized using Aegle

marmelos leaf extract exhibits excellent visible-light-driven photocatalytic removal of 4-nitroaniline and methyl orange. *Photochemical & Photobiological Sciences*, *21*(8), 1357–1370.

Bekru, A. G., Tufa, L. T., Zelekew, O. A., Goddati, M., Lee, J., & Sabir, F. K. (2022). Green Synthesis of a CuO–ZnO Nanocomposite for Efficient Photodegradation of Methylene Blue and Reduction of 4-Nitrophenol. *ACS Omega*, *7*(35), 30908–30919.

Bisht, N., More, P., Khanna, P. K., Abolhassani, R., Mishra, Y. K., & Madsen, M. (2021). Progress of hybrid nanocomposite materials for thermoelectric applications. *Materials Advances*, *2*(6), 1927–1956.

Bordbar, M., Negahdar, N., & Nasrollahzadeh, M. (2018). Melissa Officinalis L. leaf extract assisted green synthesis of CuO/ZnO nanocomposite for the reduction of 4-nitrophenol and Rhodamine B. *Separation and Purification Technology*, *191*, 295–300.

Carnat, A., Heitz, A., Fraisse, D., Carnat, A.-P., & Lamaison, J.-L. (2000). Major dicaffeoylquinic acids from Artemisia vulgaris. *Fitoterapia*, *71*(5), 587–589.

Chabri, S., Dhara, A., Show, B., Adak, D., Sinha, A., & Mukherjee, N. (2016). Mesoporous CuO–ZnO p–n heterojunction based nanocomposites with high specific surface area for enhanced photocatalysis and electrochemical sensing. *Catalysis Science & Technology*, *6*(9), 3238–3252.

Chang, T., Li, Z., Yun, G., Jia, Y., & Yang, H. (2013). Enhanced photocatalytic activity of ZnO/CuO nanocomposites synthesized by hydrothermal method. *Nano-Micro Letters*, *5*, 163–168.

Chen, C., Liu, X., Fang, Q., Chen, X., Liu, T., & Zhang, M. (2020). Self-assembly synthesis of CuO/ZnO hollow microspheres and their photocatalytic performance under natural sunlight. *Vacuum*, *174*, 109198.

Coopoosamy, S. O. O. R. M. (2015). Preliminary studies on the antibacterial and antioxidative potentials of hydroalcoholic extract from the whole parts of Artemisia vulgaris L. *Int. J. Pharm.*, *11*, 561–569.

Corrêa-Ferreira, M. L., Noleto, G. R., & Petkowicz, C. L. O. (2014). Artemisia absinthium and Artemisia vulgaris: A comparative study of infusion polysaccharides. *Carbohydrate Polymers*, *102*, 738–745.

Daphne, J., Francis, A., Mohanty, R., Ojha, N., & Das, N. (2018). Green synthesis of antibacterial silver nanoparticles using yeast isolates and its characterization. *Research Journal of Pharmacy and Technology*, *11*(1), 83–92.

Das, S., & Srivastava, V. C. (2018). An overview of the synthesis of CuO-ZnO nanocomposite for environmental and other applications. *Nanotechnology Reviews*, *7*(3), 267–282.

Ebrahiminezhad, A., Taghizadeh, S., Berenjian, A., Rahi, A., & Ghasemi, Y. (2016). Synthesis and characterization of silver nanoparticles with natural carbohydrate capping using Zataria multiflora. *Advanced Materials Letters*, *7*(11), 939–944.

Feynman, R. P. (1960). *There's Plenty of Room at the Bottom, Engineering and Science 23*.

Fouda, A., Salem, S. S., Wassel, A. R., Hamza, M. F., & Shaheen, T. I. (2020). Optimization of green biosynthesized visible light active CuO/ZnO nano-photocatalysts for the degradation of organic methylene blue dye. *Heliyon*, *6*(9), e04896.

Geissman, T. A., & Ellestad, G. A. (1962). Vulgarin, a Sesquiterpene Lactone from Artemisia vulgaris L. *The Journal of Organic Chemistry*, *27*(5), 1855–1859.

Goyal, R. K. (2017). *Nanomaterials and nanocomposites: Synthesis, properties, characterization techniques, and applications*. CRC Press.

Iijima, S. (1991). Helical microtubules of graphitic carbon. *Nature*, *354*(6348), 56–58.

Ivanescu, B., Miron, A., & Corciova, A. (2015). Sesquiterpene lactones from Artemisia genus: Biological activities and methods of analysis. *Journal of Analytical Methods in Chemistry*, *2015*.

Ivanescu, B., Vlase, L., Corciova, A., & Lazar, M. I. (2010). HPLC-DAD-MS study of polyphenols from Artemisia absinthium, A. annua, and A. vulgaris. *Chemistry of Natural Compounds*, *46*, 468–470.

Kalia, A., Kaur, M., Shami, A., Jawandha, S. K., Alghuthaymi, M. A., Thakur, A., & Abd-Elsalam, K. A. (2021). Nettle-Leaf extract derived ZnO/CuO nanoparticle-biopolymer-based antioxidant and antimicrobial nanocomposite packaging films and their impact on extending the post-harvest shelf life of guava fruit. *Biomolecules*, *11*(2), 224.

Karabegović, I., Nikolova, M., Veličković, D., Stojičević, S., Veljković, V., & Lazić, M. (2011). Comparison of antioxidant and antimicrobial activities of

methanolic extracts of the Artemisia sp. Recovered by different extraction techniques. *Chinese Journal of Chemical Engineering*, *19*(3), 504–511.

Karki, N., Neupane, S., Kumar Gupta, D., & Prasad Yadav, A. (2023). Electrochemical study on the effect of polar and non-polar extract of Artemisia vulgaris on the corrosion inhibition of mild-steel in an acidic medium. *RSC Advances*, *13*(11), 7603–7613. https://doi.org/10.1039/D3RA00148B

Karnati, P., Haque, A., Taufique, M. F. N., & Ghosh, K. (2018). A systematic study on the structural and optical properties of vertically aligned zinc oxide nanorods grown by high pressure assisted pulsed laser deposition technique. *Nanomaterials*, *8*(2), 62.

Khan, M., Shaik, M. R., Adil, S. F., Khan, S. T., Al-Warthan, A., Siddiqui, M. R. H., Tahir, M. N., & Tremel, W. (2018). Plant extracts as green reductants for the synthesis of silver nanoparticles: Lessons from chemical synthesis. *Dalton Transactions*, *47*(35), 11988–12010.

Khan, S. A., Noreen, F., Kanwal, S., Iqbal, A., & Hussain, G. (2018). Green synthesis of ZnO and Cu-doped ZnO nanoparticles from leaf extracts of Abutilon indicum, Clerodendrum infortunatum, Clerodendrum inerme and investigation of their biological and photocatalytic activities. *Materials Science and Engineering: C*, *82*, 46–59.

Khanchandani, S., Kundu, S., Patra, A., & Ganguli, A. K. (2012). Shell thickness dependent photocatalytic properties of ZnO/CdS core–shell nanorods. *The Journal of Physical Chemistry C*, *116*(44), 23653–23662.

Kolahalam, L. A., Viswanath, I. K., Diwakar, B. S., Govindh, B., Reddy, V., & Murthy, Y. L. N. (2019). Review on nanomaterials: Synthesis and applications. *Materials Today: Proceedings*, *18*, 2182–2190.

Kouhbanani, M. A. J., Beheshtkhoo, N., Amani, A. M., Taghizadeh, S., Beigi, V., Bazmandeh, A. Z., & Khalaf, N. (2018). Green synthesis of iron oxide nanoparticles using Artemisia vulgaris leaf extract and their application as a heterogeneous Fenton-like catalyst for the degradation of methyl orange. *Materials Research Express*, *5*(11), 115013.

Kroto, H. W., Heath, J. R., O'Brien, S. C., Curl, R. F., & Smalley, R. E. (1985). C60: Buckminsterfullerene. *Nature*, *318*(6042), 162–163.

Lathasree, S., Rao, A. N., SivaSankar, B., Sadasivam, V., & Rengaraj, K. (2004). Heterogeneous photocatalytic mineralisation of phenols in aqueous solutions. *Journal of Molecular Catalysis A: Chemical*, *223*(1–2), 101–105.

Lee, S.-J., Chung, H.-Y., Lee, I.-K., & Yoo, I.-D. (1999). Isolation and identification of flavonoids from ethanol extracts of Artemisia vulgaris and their antioxidant activity. *Korean Journal of Food Science and Technology*, *31*(3), 815–822.

Lee, S.-J., Chung, H.-Y., Maier, C. G.-A., Wood, A. R., Dixon, R. A., & Mabry, T. J. (1998). Estrogenic flavonoids from Artemisia vulgaris L. *Journal of Agricultural and Food Chemistry*, *46*(8), 3325–3329.

Li, G., Zhang, K., Mezaal, M. A., Zhang, R., & Lei, L. (2015). Effect of electrolyte concentration and depth of discharge for zinc-air fuel cell. *Int. J. Electrochem. Sci*, *10*, 6672–6683.

Li, X., Dong, Q., Tian, Q., Sial, A., Wang, H., Wen, H., Pan, B., Zhang, K., Qin, J., & Wang, C. (2022). Recent advance in metal-and covalent-organic framework-based photocatalysis for hydrogen evolution. *Materials Today Chemistry*, *26*, 101037.

Mansournia, M., & Ghaderi, L. (2017). CuO@ZnO core-shell nanocomposites: Novel hydrothermal synthesis and enhancement in photocatalytic property. *Journal of Alloys and Compounds*, *691*, 171–177. https://doi.org/10.1016/j.jallcom.2016.08.267

Mansournia, M., Rafizadeh, S., & Hosseinpour-Mashkani, S. M. (2016). An ammonia vapor-based approach to ZnO nanostructures and their study as photocatalyst material. *Ceramics International*, *42*(1), 907–916.

Marco, J. A., Sanz, J. F., & Del Hierro, P. (1991). Two eudesmane acids from Artemisia vulgaris. *Phytochemistry*, *30*(7), 2403–2404.

Marslin, G., Siram, K., Maqbool, Q., Selvakesavan, R. K., Kruszka, D., Kachlicki, P., & Franklin, G. (2018). Secondary metabolites in the green synthesis of metallic nanoparticles. *Materials*, *11*(6), 940.

Melguizo-Melguizo, D., Diaz-de-Cerio, E., Quirantes-Piné, R., Švarc-Gajić, J., & Segura-Carretero, A. (2014). The potential of Artemisia vulgaris leaves as a source of antioxidant phenolic compounds. *Journal of Functional Foods*, *10*, 192–200.

Merugu, R., Gothalwal, R., Deshpande, P. K., De Mandal, S., Padala, G., & Chitturi, K. L. (2021). Synthesis of Ag/Cu and Cu/Zn bimetallic nanoparticles using

toddy palm: Investigations of their antitumor, antioxidant and antibacterial activities. *Materials Today: Proceedings*, *44*, 99–105.

Minal, S. P., & Prakash, S. (2016). Cu-Zn and Ag-Cu bimetallic nanoparticles as larvicide to control malaria parasite vector: A comparative analysis. *2016 IEEE Region 10 Humanitarian Technology Conference (R10-HTC)*, 1–6.

Mohammadi-Aloucheh, R., Habibi-Yangjeh, A., Bayrami, A., Latifi-Navid, S., & Asadi, A. (2018). Enhanced anti-bacterial activities of ZnO nanoparticles and ZnO/CuO nanocomposites synthesized using Vaccinium arctostaphylos L. fruit extract. *Artificial Cells, Nanomedicine, and Biotechnology*, *46*(sup1), 1200–1209.

Natividad, G. M., Broadley, K. J., Kariuki, B., Kidd, E. J., Ford, W. R., & Simons, C. (2011). Actions of Artemisia vulgaris extracts and isolated sesquiterpene lactones against receptors mediating contraction of guinea pig ileum and trachea. *Journal of Ethnopharmacology*, *137*(1), 808–816.

Nguyen, H. T. T., Nguyen, H. T., Islam, M. Z., Obi, T., Pothinuch, P., Zar, P. P. K., Van Nguyen, T., Nguyen, T. M., Van Dao, C., & Shiraishi, M. (2016). Pharmacological characteristics of Artemisia vulgaris L. in isolated porcine basilar artery. *Journal of Ethnopharmacology*, *182*, 16–26.

Nikolova, M., Gevrenova, R., & Ivancheva, S. (2004). High-performance liquid chromatographic separation of surface flavonoid aglycones in Artemistia annua L. and Artemisia vulgaris L. *Journal of the Serbian Chemical Society*, *69*(7), 571–574.

Nikolova, M. T., & Ivancheva, S. V. (2005). Quantitative flavonoid variations of Artemisia vulgaris L. and Veronica chamaedrys L. in relation to altitude and polluted environment. *Acta Biologica Szegediensis*, *49*(3–4), 29–32.

Nikolova, M., & VELICKOVIC, D. (2007). Phenological Variations in the Surface Flavonoids of Artemisia vulgaris L. and Artemisia absinthium L. *Turkish Journal of Botany*, *31*(5), 459–462.

Pandey, S., Mewada, A., Thakur, M., Shah, R., Oza, G., & Sharon, M. (2013). Biogenic gold nanoparticles as fotillas to fire berberine hydrochloride using folic acid as molecular road map. *Materials Science and Engineering: C*, *33*(7), 3716–3722.

Pandya, S., Jani, S., Chavan, A., Singh, A. K., Bhatt, S., Patel, D., Bhatt, B., Patel, A., Girma, A., & Naik, K. (2013). Nanocomposites and IT'S application-review. *Int J Pharm Sci Res*, *4*(1), 19–28.

Pires, J. M., Mendes, F. R., Negri, G., Duarte-Almeida, J. M., & Carlini, E. A. (2009). Antinociceptive peripheral effect of Achillea millefolium L. and Artemisia vulgaris L.: Both plants known popularly by brand names of analgesic drugs. *Phytotherapy Research: An International Journal Devoted to Pharmacological and Toxicological Evaluation of Natural Product Derivatives*, *23*(2), 212–219.

Qamar, M. T., Aslam, M., Ismail, I. M., Salah, N., & Hameed, A. (2015). Synthesis, characterization, and sunlight mediated photocatalytic activity of CuO coated ZnO for the removal of nitrophenols. *ACS Applied Materials & Interfaces*, *7*(16), 8757–8769.

Qi, K., Xing, X., Zada, A., Li, M., Wang, Q., Liu, S., Lin, H., & Wang, G. (2020). Transition metal doped ZnO nanoparticles with enhanced photocatalytic and antibacterial performances: Experimental and DFT studies. *Ceramics International*, *46*(2), 1494–1502.

Reshmy, R., Philip, E., Sirohi, R., Tarafdar, A., Arun, K. B., Madhavan, A., Binod, P., Awasthi, M. K., Varjani, S., & Szakacs, G. (2021). Nanobiocatalysts: Advancements and applications in enzyme technology. *Bioresource Technology*, *337*, 125491.

Roy, A. (2017). Synthesis of silver nanoparticles from medicinal plants and its biological application: A review. *Research & Reviews in BioSciences*, *12*(4), 138.

Sakib, A. A. M., Masum, S. M., Hoinkis, J., Islam, R., & Molla, M. A. I. (2019). Synthesis of CuO/ZnO nanocomposites and their application in photodegradation of toxic textile dye. *Journal of Composites Science*, *3*(3), 91.

Saraji, M., Khayamian, T., Hashemian, Z., Aslipashaki, S. N., & Talebi, M. (2013). Determination of artemisinin in Artemisia species by hollow fiber-based liquid-phase microextraction and electrospray ionization-ion mobility spectrometry. *Analytical Methods*, *5*(16), 4190–4195.

Shanmuganathan, R., MubarakAli, D., Prabakar, D., Muthukumar, H., Thajuddin, N., Kumar, S. S., & Pugazhendhi, A. (2018). An enhancement of antimicrobial

efficacy of biogenic and ceftriaxone-conjugated silver nanoparticles: Green approach. *Environmental Science and Pollution Research*, *25*, 10362–10370.

Sherly, E. D., Vijaya, J. J., & Kennedy, L. J. (2015). Visible-light-induced photocatalytic performances of ZnO–CuO nanocomposites for degradation of 2, 4-dichlorophenol. *Chinese Journal of Catalysis*, *36*(8), 1263–1272.

Silverstein, R. M., & Bassler, G. C. (1962). Spectrometric identification of organic compounds. *Journal of Chemical Education*, *39*(11), 546.

Smura, C. F., Parker, D. R., Zbiri, M., Johnson, M. R., Gál, Z. A., & Clarke, S. J. (2011). High-spin cobalt (II) ions in square planar coordination: Structures and magnetism of the oxysulfides Sr2CoO2Cu2S2 and Ba2CoO2Cu2S2 and their solid solution. *Journal of the American Chemical Society*, *133*(8), 2691–2705.

Sugiyama, M. (2015). Historical review of research on plant cell dedifferentiation. *Journal of Plant Research*, *128*, 349–359.

Tahvilian, R., Zangeneh, M. M., Falahi, H., Sadrjavadi, K., Jalalvand, A. R., & Zangeneh, A. (2019). Green synthesis and chemical characterization of copper nanoparticles using Allium saralicum leaves and assessment of their cytotoxicity, antioxidant, antimicrobial, and cutaneous wound healing properties. *Applied Organometallic Chemistry*, *33*(12), e5234.

Taufique, M. F. N., Haque, A., Karnati, P., & Ghosh, K. (2018). ZnO–CuO nanocomposites with improved photocatalytic activity for environmental and energy applications. *Journal of Electronic Materials*, *47*, 6731–6745.

Thangjam, N. M., Taijong, J., & Kumar, A. (2020). Phytochemical and pharmacological activities of methanol extract of Artemisia vulgaris L. leaves. *Clinical Phytoscience*, *6*(1), 1–8.

Thatikayala, D., & Min, B. (2021). Ginkgo leaves extract-assisted synthesis of ZnO/CuO nanocrystals for efficient UV-induced photodegradation of organic dyes and antibacterial activity. *Journal of Materials Science: Materials in Electronics*, *32*(13), 17154–17169.

Tigno, X. T., de Guzman, F., Flora, A. M., & Theresa, V. (2000). Phytochemical analysis and hemodynamic actions of Artemisia vulgaris L. *Clinical Hemorheology and Microcirculation*, *23*(2, 3, 4), 167–175.

Tolochko, N. K. (2009). History of nanotechnology. *Encyclopedia of Life Support Systems (EOLSS)*.

Wang, J., Fan, X. M., Wu, D. Z., Dai, J., Liu, H., Liu, H. R., & Zhou, Z. W. (2011). Fabrication of CuO/T-ZnOw nanocomposites using photo-deposition and their photocatalytic property. *Applied Surface Science*, *258*(5), 1797–1805.

Weston, L. A., Barney, J. N., & DiTommaso, A. (2005). A review of the biology and ecology of three invasive perennials in New York State: Japanese knotweed (Polygonum cuspidatum), mugwort (Artemisia vulgaris) and pale swallow-wort (Vincetoxicum rossicum). *Plant and Soil*, *277*, 53–69.

Xu, L., Zhou, Y., Wu, Z., Zheng, G., He, J., & Zhou, Y. (2017). Improved photocatalytic activity of nanocrystalline ZnO by coupling with CuO. *Journal of Physics and Chemistry of Solids*, *106*, 29–36.

Xu, S., Qin, Y., Xu, C., Wei, Y., Yang, R., & Wang, Z. L. (2010). Self-powered nanowire devices. *Nature Nanotechnology*, *5*(5), 366–373.

Yulizar, Y., Bakri, R., Apriandanu, D. O. B., & Hidayat, T. (2018). ZnO/CuO nanocomposite prepared in one-pot green synthesis using seed bark extract of Theobroma cacao. *Nano-Structures & Nano-Objects*, *16*, 300–305.

Supplementary

Table-S1: Various phytochemical present in *Artemisia vulgaris*

Class	Compounds	Parts of plant	Reference
Flavonoid	apigenin	leaf	Karabegović et al., 2011.
	chrysoeriol	Whole plant	Lee et al., 1998, 1999
	diosmetin	Whole plant	Lee et al., 1998, 1999
	eriodictyol	Whole plant	Lee et al., 1998, 1999
	eupafolin	Whole plant	Lee et al., 1998, 1999
	homoeriodictyol	Whole plant	Lee et al., 1998, 1999
	isoquercitrin	Aerial part	Ivanescu et al., 2010
	isorhamnetin	whole plant	Lee et al., 1998, 1999; Ivanescu et al., 2015
	jaceosidine	whole plant	Lee et al., 1998, 1999
	kaempferol 3,7-dimethyl ether	Aerial part	M. T. Nikolova & Ivancheva, 2005;Nikolova & VELICKOVIC, 2007;M. Nikolova et al., 2004
	kaempferol	Aerial part	Ivanescu et al., 2010
	kaempferol-3-glucoside	leaf	Melguizo-Melguizo et al., 2014
	kaempferol 3-rutinoside	whole plant	Lee et al., 1998, 1999
	kaempferol 7-glucoside	whole plant	Lee et al., 1998, 1999
	Luteolin	Aerial part	Ivanescu et al., 2010
	Luteolin 7-glucoside	whole plant	Lee et al., 1998, 1999
	Luteolin rutinoside	leaf	Melguizo-Melguizo et al., 2014
	chrysosplenetin	Aerial part	M. Nikolova et al., 2004
	artemetin	Aerial part	M. Nikolova et al., 2004; Nikolova & VELICKOVIC, 2007
	quercetin	Aerial part	Nikolova & VELICKOVIC, 2007; Ivanescu et al., 2010
	quercetin 3,3'-dimethyl ether	Aerial part, leaf	Karabegović et al., 2011; M. Nikolova et al., 2004; M. Nikolova & VELICKOVIC, 2007
	quercetin 3,7,3'-trimethyl ether	Aerial part, leaf	Karabegović et al., 2011; M. Nikolova et al., 2004;

			M. T. Nikolova & Ivancheva, 2005; M. Nikolova & VELICKOVIC, 2007
	quercetin 3,7-dimethyl ether	Aerial part, leaf	Karabegović et al., 2011; M. Nikolova & VELICKOVIC, 2007
	quercetin 3-galactoside	Leaf, whole plant	Karabegović et al., 2011; Lee et al., 1998, 1999; Melguizo-Melguizo et al., 2014
	quercetin 3-glucoside	whole plant	Lee et al., 1998, 1999
	quercetin 7-glucoside	whole plant	Lee et al., 1998, 1999
	quercetin-3-malonylglucoside	leaf	Melguizo-Melguizo et al., 2014
	quercetrin	Aerial part, whole plant	Ivanescu et al., 2010; Lee et al., 1998, 1999
	rutin	Aerial part,leaf, whole plant	Coopoosamy, 2015; Ivanescu et al., 2010; Lee et al., 1998, 1999; Melguizo-Melguizo et al., 2014; Pires et al., 2009
	tricine	whole plant	Lee et al., 1998, 1999
	vitexin	whole plant	Lee et al., 1998, 1999
phenolic acid	1,3-O-dicaffeoylquinic acid/1,4-Odicaff	Leaf	Melguizo-Melguizo et al., 2014
	1,5-O-dicaffeoylquinic acid	flowering tops, Leaf	Carnat et al., 2000; Melguizo-Melguizo et al., 2014
	3,4-O-dicaffeoylquinic acid	Leaf	Melguizo-Melguizo et al., 2014
	3,5-O-dicaffeoylquinic acid	flowering tops, Leaf	Carnat et al., 2000; Melguizo-Melguizo et al., 2014
	3-O-caffeoylquinic acid	Leaf	Melguizo-Melguizo et al., 2014
	4,5-O-dicaffeoylquinic acid	Leaf	Melguizo-Melguizo et al., 2014
	5-O-caffeoylquinic acid	Aerial part, Leaf	Ivanescu et al., 2010;

			Melguizo-Melguizo et al., 2014
	5-O-feruloylquinic acid	Leaf	Melguizo-Melguizo et al., 2014
	gallic acid	whole plant	Coopoosamy, 2015
	protocatechuic acid glucoside	Leaf	Melguizo-Melguizo et al., 2014
organic acid	malic acid	Leaf	Melguizo-Melguizo et al., 2014
	quinic acid	Leaf	Melguizo-Melguizo et al., 2014
	trihydroxy-octadecenoic acid	Leaf	Melguizo-Melguizo et al., 2014
	tuberonic acid glucoside	Leaf	Melguizo-Melguizo et al., 2014
sesquiterpene	artemisinin	Lleaf, stem and root	Saraji et al., 2013
	eudesmane dialcohol	Aerial part	Marco et al., 1991
	new sesquiterpene 1	Leaf	Ragasa et al., 2008
sesquiterpenic acid	3-oxoeudesma-1,4,11(13)-trien-7αH-12-oic acid	Aerial part	Marco et al., 1991
	lα-hydroxyeudesma-2,4(15),11(13)- trien-5α,7αH-12-oic acid	Aerial part	Marco et al., 1991
sesquiterpene glucoside	artemisinic acid glucoside isomer 1	Leaf	Melguizo-Melguizo et al., 2014
	artemisinic acid glucoside isomer 2	Leaf	Melguizo-Melguizo et al., 2014
sesquiterpene lactone	1,2,3,4-diepoxy-11(13) eudesmen12,8-olide	leaf	Natividad et al., 2011; Tigno et al., 2000
	vulgarin	whole plant	Geissman & Ellestad, 1962
	yomogin	Leaf	Natividad et al., 2011; Tigno et al., 2000
ignan glucoside	tracheloside	Leaf	Melguizo-Melguizo et al., 2014
monoterpene	dehydrovomifoliol	Leaf	Melguizo-Melguizo et al., 2014
monoamine neurotransmitter	5-HT,5- hydroxytryptamine	Leaf	Nguyen et al., 2016

Table-S2: Phytochemical Analysis Protocol

S.N.	Experiment	Observation	Inference
1	Test for alkaloids a. Mayer's test 3 drops of Mayer's reagent+ 2 mL of extract, shake well	Yellowish ppt.	Presence of alkaloids
	b. Dragendorff's test 3 drops Dragendorff's reagent+ 2 mL extract, shake well	Yellowish ppt.	Presence of alkaloids
2	Test for flavonoids 5 mL dil. Ammonia solution+ extract+ conc. Sulphuric acidfrom side of the tube	Yellow color	Presence of flavonoids
3	Test for terpenoids 2 mL $CHCL_3$ + 5 mL extract + 3 mL conc. H_2SO_4 slowly	Reddish brown color	Presence of terpenoids
4	Test for saponins 5 mL extract + 20 mL distilled water, shake vigorously	Appearance of frothing	Presence of saponins
5	Test for quinones 2 mL extract + Conc. HCl	Yellow colored ppt.	Presence of quinones
6	Test for polyphenols 3 drops of 5 % $FeCl_3$ + 2 mL extract, shake	Black color	Presence of polyphenols
7	Test for glycosides 3 drops of Molish's reagent + 2 mL extract, shake well + few drops Conc. H_2SO_4 slowly from the side tube and allow to stand for few minutes	Violet ring at junction of two layers	Presence of glycosides
8	Test for proteins Biuret Test: 2 mL 5 % NaOH + 2 mL extract + $CuSO_4$ solution	Pink color	Presence of proteins